

Accelerated Article Preview

Clofazimine broadly inhibits coronaviruses including SARS-CoV-2

Received: 30 September 2020

Accepted: 8 March 2021

Accelerated Article Preview Published
online 16 March 2021

Cite this article as: Yuan, S. et al. Clofazimine broadly inhibits coronaviruses including SARS-CoV-2. *Nature* <https://doi.org/10.1038/s41586-021-03431-4> (2021).

Shuofeng Yuan, Xin Yin, Xiangzhi Meng, Jasper Fuk-Woo Chan, Zi-Wei Ye, Laura Riva, Lars Pache, Chris Chun-Yiu Chan, Pok-Man Lai, Chris Chung-Sing Chan, Vincent Kwok-Man Poon, Andrew Chak-Yiu Lee, Naoko Matsunaga, Yuan Pu, Chun-Kit Yuen, Jianli Cao, Ronghui Liang, Kaiming Tang, Li Sheng, Yushen Du, Wan Xu, Chit-Ying Lau, Ko-Yung Sit, Wing-Kuk Au, Runming Wang, Yu-Yuan Zhang, Yan-Dong Tang, Thomas Mandel Clausen, Jessica Pihl, Juntaek Oh, Kong-Hung Sze, Anna Jinxia Zhang, Hin Chu, Kin-Hang Kok, Dong Wang, Xue-Hui Cai, Jeffrey D. Esko, Ivan Fan-Ngai Hung, Ronald Adolphus Li, Honglin Chen, Hongzhe Sun, Dong-Yan Jin, Ren Sun, Sumit K. Chanda & Kwok-Yung Yuen

This is a PDF file of a peer-reviewed paper that has been accepted for publication. Although unedited, the content has been subjected to preliminary formatting. Nature is providing this early version of the typeset paper as a service to our authors and readers. The text and figures will undergo copyediting and a proof review before the paper is published in its final form. Please note that during the production process errors may be discovered which could affect the content, and all legal disclaimers apply.

Clofazimine broadly inhibits coronaviruses including SARS-CoV-2

<https://doi.org/10.1038/s41586-021-03431-4>

Received: 30 September 2020

Accepted: 8 March 2021

Published online: 16 March 2021

Shuofeng Yuan^{1,2,3,19}, Xin Yin^{4,5,19}, Xiangzhi Meng^{2,19}, Jasper Fuk-Woo Chan^{3,6,19}, Zi-Wei Ye^{2,19}, Laura Riva^{5,18}, Lars Pache⁵, Chris Chun-Yiu Chan², Pok-Man Lai², Chris Chung-Sing Chan², Vincent Kwok-Man Poon², Andrew Chak-Yiu Lee², Naoko Matsunaga⁵, Yuan Pu⁵, Chun-Kit Yuen², Jianli Cao², Ronghui Liang², Kaiming Tang², Li Sheng^{7,8}, Yushen Du⁸, Wan Xu⁷, Chit-Ying Lau⁷, Ko-Yung Sit⁹, Wing-Kuk Au⁹, Runming Wang¹⁰, Yu-Yuan Zhang⁴, Yan-Dong Tang⁴, Thomas Mandel Clausen^{11,12}, Jessica Pihl^{11,13}, Juntaek Oh^{11,14}, Kong-Hung Sze^{1,2}, Anna Jinxia Zhang^{1,2}, Hin Chu^{1,2}, Kin-Hang Kok^{1,2}, Dong Wang^{11,14}, Xue-Hui Cai⁴, Jeffrey D. Esko^{11,15}, Ivan Fan-Ngai Hung¹⁶, Ronald Adolphus Li¹⁷, Honglin Chen^{1,2}, Hongzhe Sun¹⁰, Dong-Yan Jin⁷, Ren Sun^{7,8}, Sumit K. Chanda^{5,18} & Kwok-Yung Yuen^{1,2,3,6}

COVID-19 pandemic is the third zoonotic coronavirus (CoV) outbreak of the century after severe acute respiratory syndrome (SARS) in 2003¹ and Middle East respiratory syndrome (MERS) since 2012². Treatment options for CoVs are largely lacking. Here we show that clofazimine, an anti-leprosy drug with a favourable safety profile³, possesses pan-coronaviral inhibitory activity, and can antagonize SARS-CoV-2 and MERS-CoV replication in multiple in vitro systems. The FDA-approved molecule was found to inhibit viral spike-mediated cell fusion and viral helicase activity. In a hamster model of SARS-CoV-2 pathogenesis, prophylactic or therapeutic administration of clofazimine significantly reduced viral load in the lung and faecal viral shedding, and also mitigated inflammation associated with viral infection. Combinatorial application of clofazimine and remdesivir exhibited antiviral synergy in vitro and in vivo, and restricted upper respiratory tract viral shedding. Since clofazimine is orally bioavailable and has a comparatively low manufacturing cost, it is an attractive clinical candidate for outpatient treatment and remdesivir-based combinatorial therapy for hospitalized COVID-19 patients, particularly in developing countries. Taken together, our data provide evidence that clofazimine may have a role in the control of the current pandemic SARS-CoV-2, and, possibly most importantly, emerging CoVs of the future.

COVID-19 in human has a broad clinical spectrum ranging from mild to severe manifestations, with a mortality rate of ~2% worldwide⁴. The high transmissibility of SARS-CoV-2 was attributed to a significant proportion of mild or asymptomatic infections^{5,6}. The genetically diverse coronavirus (CoV) family, currently composed of four genera (α , β , γ , and δ), infects birds, bats and a variety of mammals⁷. Within two decades, the world's human population has undergone three

major CoV outbreaks. SARS-CoV-1 emerged in Guangdong, China in 2002 and, with the aid of commercial air travel, spread rapidly and globally, causing more than 8,000 cases with 10% mortality¹. In 2012, MERS-CoV may have evolved and spread from bats to humans through an intermediate camel host, causing over 1,700 cases with almost 40% mortality, and, like SARS-CoV-1, air travel has enabled global spread to 27 countries^{2,8}.

¹State Key Laboratory of Emerging Infectious Diseases, Li Ka Shing Faculty of Medicine, The University of Hong Kong, Pokfulam, Hong Kong Special Administrative Region, China.

²Department of Microbiology, Li Ka Shing Faculty of Medicine, The University of Hong Kong, Pokfulam, Hong Kong Special Administrative Region, China. ³Department of Clinical Microbiology and Infection Control, The University of Hong Kong-Shenzhen Hospital, Shenzhen, Guangdong Province, China. ⁴State Key Laboratory of Veterinary Biotechnology, Harbin Veterinary Research Institute, Chinese Academy of Agricultural Sciences, Harbin, China. ⁵Immunity and Pathogenesis Program, Infectious and Inflammatory Disease Center, Sanford Burnham Prebys Medical Discovery Institute, La Jolla, CA, USA. ⁶Hainan Medical University-The University of Hong Kong Joint Laboratory of Tropical Infectious Diseases, Hainan Medical University, Haikou, Hainan, and The University of Hong Kong, Pokfulam, Hong Kong Special Administrative Region, China. ⁷School of Biomedical Sciences, Li Ka Shing Faculty of Medicine, The University of Hong Kong, Pokfulam, Hong Kong Special Administrative Region, China. ⁸Department of Molecular and Medical Pharmacology, David Geffen School of Medicine, University of California Los Angeles, Los Angeles, CA, USA. ⁹Department of Surgery, The University of Hong Kong, Queen Mary Hospital, Pokfulam, Hong Kong Special Administrative Region, China. ¹⁰Department of Chemistry, State Key Laboratory of Synthetic Chemistry, CAS-HKU Joint Laboratory of Metallomics on Health and Environment, The University of Hong Kong, Pokfulam, Hong Kong Special Administrative Region, China. ¹¹Department of Cellular and Molecular Medicine, University of California, San Diego, La Jolla, CA, USA. ¹²Copenhagen Center for Glycomics, Department of Molecular and Cellular Medicine, Faculty of Health and Medical Sciences, University of Copenhagen, Copenhagen, Denmark. ¹³Department of Immunology and Microbiology, Faculty of Health and Medical Sciences, University of Copenhagen, Copenhagen, Denmark. ¹⁴Division of Pharmaceutical Sciences, Skaggs School of Pharmacy and Pharmaceutical Sciences, University of California San Diego, La Jolla, CA, USA. ¹⁵Glycobiology Research and Training Center, University of California, San Diego, La Jolla, CA, USA. ¹⁶Department of Medicine, Li Ka Shing Faculty of Medicine, The University of Hong Kong, Pokfulam, Hong Kong Special Administrative Region, China. ¹⁷Ming Wai Lau Centre for Reproductive Medicine, Karolinska Institutet, and Dr. Li Dak-Sum Research Centre, The University of Hong Kong, Pokfulam, Hong Kong Special Administrative Region, China. ¹⁸Present address: Calibr at Scripps Research, La Jolla, CA, USA. ¹⁹These authors contributed equally: Shuofeng Yuan, Xin Yin, Xiangzhi Meng, Jasper Fuk-Woo Chan, Zi-Wei Ye. ✉e-mail: rensun@hku.hk; schanda@sbpdiscovery.org; kyyuen@hku.hk

Currently, there are no widely available specific antiviral therapies for CoV in humans⁹. Remdesivir exhibited pan-coronavirus inhibitory potential¹⁰, and was granted approval by the FDA for the treatment of COVID-19 based on the reduced time to recovery¹¹. However, the therapy is suboptimal, particularly for severe COVID-19 patients, and can only be administered intravenously to hospitalized patients^{12,13}. Thus, development of additional therapeutic options is urgent, as well as the establishment of combinatorial regimens to improve efficacy and reduce the potential for the emergence of drug resistant variants. For example, the triple antiviral combination of interferon beta-1b, lopinavir–ritonavir, and ribavirin, has been shown to be beneficial in a randomized clinical trial¹⁴.

In efforts to accelerate the development of novel therapies for COVID-19, we previously profiled a library of known drugs encompassing approximately 12,000 clinical-stage or FDA-approved small molecules¹⁵. In this study, we focus on the antiviral mechanisms of action and *in vivo* efficacy of clofazimine, an FDA-approved molecule discovered as an anti-tuberculosis drug and later used for treatment of leprosy¹⁶. The effective concentration of clofazimine against SARS-CoV-2 *in vitro* (EC_{50} 0.31 μ M in VeroE6 cells) is clinically achievable with a single dose of 200 mg/man/day (C_{max} 0.86 μ M)¹⁷. Sufficiently high concentration of clofazimine, as multiples of its $EC_{90.5}$ in different cell lines (EC_{90} 0.81–2.35 μ M), is known to accumulate in plasma and lung tissue after multiple dosing¹⁸. Here, we report the protective effect of clofazimine against SARS-CoV-2 and MERS-CoV infection in primary human cells and animal model. Most importantly, clofazimine is affordable by COVID-19 patients in developing countries, which may substantially be relieved of the acute healthcare burden created by this continuing pandemic¹⁹.

Clofazimine is a pan-coronavirus inhibitor

Clofazimine reduced MERS-CoV replication in VeroE6 cells with an EC_{50} of 1.48 \pm 0.17 μ M (Extended Data Figure 1a). Immunofluorescence staining for MERS-CoV-N protein and flow cytometry analysis illustrated effective suppression of virus infection in human hepatocellular Huh7 cells upon clofazimine treatment (Extended Data Figure 1b). We then characterized the antiviral activity of clofazimine in two more physiologically relevant: human embryonic stem cell-derived cardiomyocytes (CM) and human primary small airway epithelial cells (HSAEpC), which robustly support SARS-CoV-2²⁰ and MERS-CoV²¹ replication, respectively. Clofazimine treatment reduced SARS-CoV-2 titer up to >3 -log₁₀ and that of MERS-CoV by 2-log₁₀ (Figure 1a). Next, we assessed the antiviral activity of clofazimine in an *ex vivo* lung culture system and found that clofazimine potently antagonized viral replication in human lung tissues that reflect the primary site of SARS-CoV-2 and MERS-CoV replication (Figure 1b). To explore whether clofazimine confers cross-protection against other epidemic and seasonal CoVs, we performed viral load reduction assays for SARS-CoV-1, hCoV-229E and hCoV-OC43 in corresponding cell lines that support virus replication. Viral yields in the cell culture supernatants were decreased by ~ 2 -log₁₀ in SARS-CoV-1-infected VeroE6 cells, by ~ 4 -log₁₀ in hCoV-229E infected-human embryonic lung fibroblasts (HELFI), and by ~ 3 -log₁₀ in hCoV-OC43-infected monkey BSC1 cells (Figure 1c). Importantly, clofazimine showed negligible cytotoxicity in the matching cell line at concentrations as described above (Extended Data Figure 1c). Overall, clofazimine exhibited broad-spectrum anti-CoV efficacy, and antagonized both SARS-CoV-2 and MERS-CoV replication in human primary cell and *ex vivo* lung models.

Effects on SARS-CoV-2 life cycle

Antiviral activity of clofazimine was first evaluated by a time-of-drug addition assay in a single infectious cycle. Treatment with clofazimine during inoculation strongly inhibited SARS-CoV-2 infection, indicating that clofazimine inhibits viral entry. Intriguingly, clofazimine also

blocked SARS-CoV-2 infection at a post-entry step as evidenced by the observed reduction of viral infection when clofazimine was added at 5hpi (Extended Data Figure 2a). To further evaluate the impact of clofazimine on viral entry, we employed vesicular stomatitis virus (VSV)-based Spike (S) pseudotyped virions. Clofazimine treatment reduced the infectivity of both SARS-CoV-1 S and SARS-CoV-2 S pseudotyped virions in VeroE6 cells whereas did not affect MERS-CoV S pseudotyped virus particles (Figure 2a). Examining a series of events to dissect the precise step of SARS-CoV-2 entry that was blocked by clofazimine, we excluded possible effects of clofazimine on: i) the cell surface expression of SARS-CoV-2 receptors angiotensin-converting enzyme 2 (ACE2) and MERS-CoV receptor dipeptidyl peptidase 4 (DPP4) (Extended Data Figure 2b) as well as ii) the disruption of binding between the ACE2 or another attachment factor heparan sulfate²² and SARS-CoV-2 spike protein (Extended Data Figure 2c). Intriguingly, using a SARS-CoV-2 spike-mediated cell membrane fusion assay^{23,24}, we find that clofazimine inhibited the spike-mediated cell fusion activity. Specifically, in a dose-dependent manner, we observed that fusion between effector cells expressing spike protein and target cells were effectively reduced after clofazimine addition (Figure 2c and Extended Data Figure 2d). To confirm whether clofazimine also inhibits post-entry steps of viral replication, we evaluated the impact of clofazimine on viral RNA production by electroporating *in vitro* transcribed viral RNA into VeroE6 cells, which bypasses clofazimine-mediated inhibition on the entry process, and directly measures RNA synthesis (Extended Data Figure 2e). As expected, remdesivir reduced the synthesis of negative-stranded RNA in a dose-dependent manner (blue symbols, Figure 2c). Intriguingly, viral RNA levels were also reduced by 1–1.5-log₁₀ in the clofazimine-treated cells (red symbols, Figure 2c). However, no significant effect was observed on electroporated GFP mRNA translation (Extended Data Figure 2f); and clofazimine was also found not to impact M^{pro} and PL^{pro} protease activity that are responsible for the cleavage of viral polypeptide ($IC_{50} > 100$ μ M, Extended Data Figure 2g). Since a critical step of SARS-CoV-2 replication/transcription requires the formation of a stable complex of nsp13 and holo-RdRp²⁵, we further investigated the effect of clofazimine on this step, and found that clofazimine inhibited the unwinding activity of SARS-CoV-2 helicase (nsp13) utilizing either dsDNA or dsRNA substrate (Figure 2d). However, clofazimine did not block the primer elongation activity executed by holo-RdRp (Extended Data Figure 2h). Collectively, these results demonstrated that clofazimine exerts antiviral activity by targeting multiple steps in SARS-CoV-2 replication, including interference with spike-mediated cell fusion, as well as viral helicase activity.

Transcriptional analysis after treatment

We employed RNA-Seq to profile the transcriptome-wide changes in SARS-CoV-2 infected human Caco-2 cells, where clofazimine exhibited comparable antiviral potency to remdesivir (Extended Data Figure 3a). Transcriptional analysis was performed in Caco-2 cells that were either infected or uninfected, and subsequently treated with clofazimine or DMSO, for 3 hours or 6 hours (Extended Data Figure 3b). At 3hpi, clofazimine treatment caused overall transcriptome shift towards mock-control group (Extended Data Figure 3c), which corroborates the drug interfering virus early life cycle. At 6hpi, there were 607 and 448 genes up- and down-regulated by SARS-CoV-2 infection, respectively (Supplementary Tables 1 and 2). The RNA level of $>90\%$ of these genes was reverted by clofazimine treatment, indicating that clofazimine treatment abrogated transcriptomic changes induced by SARS-CoV-2 infection. This is consistent with PCA of the dataset which shows that treatment with clofazimine at 6hpi caused a dramatic shift towards mock (Extended Data Figures 3c and 3d). Interestingly, clofazimine treatment for 6 hours in the absence of infection up-regulated the expression of transcription factors critical for immediate-early cellular response, including AP-1, SMAD and MAFF families (Extended

Data Figures 3e). When clofazimine was applied onto infected cells for 6 hours, we observed an enrichment of upregulated genes associated with innate immunity-related pathways, including MAPK, interleukin and TNF responses (Extended Data Figures 3f, 4a and 4b). These results suggest that clofazimine may also rewire the transcriptional landscape to prime the innate immunity-related pathways.

Prophylactic and therapeutic activities *in vivo*

Previous pharmacokinetics studies revealed that co-administration of a 200mg/human dose of clofazimine with food resulted in a C_{max} of 0.41mg/L (equivalent to 0.86 μ M) with a T_{max} of 8h. Here, we employed a golden Syrian hamster model²⁶ to determine the *in vivo* antiviral efficacy of clofazimine. Since administration of clofazimine with a high-fat meal provides better bioavailability²⁷, we delivered the drug through oral route utilizing corn oil as vehicle (Figure 3a).

After clofazimine administration, a reduction in body weight loss was observed in prophylactic regimen. Clofazimine given post-virus-challenge also shortened the time of body weight rebound (Figure 3b and 3c). At 4dpi when viral loads peaked with significant histopathological changes, clofazimine decreased virus plaque forming units in lung tissues by -1 to 2-log₁₀ (Figure 3d). Consistently, suppression of SARS-CoV-2 viral genome copies in the lungs were confirmed in the clofazimine-treated hamsters (Extended Data Figure 5a). In addition, the capacity of clofazimine to diminish SARS-CoV-2 shedding was evaluated in nasal wash and fecal samples. At 4dpi after remdesivir or clofazimine therapy, no significant reduction of infectious virus titer was detected in the hamster nasal wash; whereas an average of 2-fold reduction was achieved with prophylactic clofazimine administration (Figure 3e). Irrespective of prophylactic or therapeutic clofazimine administration, significantly lower viral loads were found in the animal feces at 4dpi when compared with the vehicle group. Remdesivir, however, did not alleviate the virus shedding from gastrointestinal tract (Figure 3f). Overall, we demonstrate *in vivo* that clofazimine antagonizes SARS-CoV-2 replication in the lung and reduced virus shedding in feces.

To ascertain if clofazimine improves the disease pathogenesis, we determined the serum IL-6 level that has been shown to correlate with respiratory failure and adverse clinical outcome²⁸. Substantially decreased serum IL-6 level was generally detected in both clofazimine and remdesivir groups (Figure 3g). It has been reported that clofazimine may inhibit lymphocyte function in cell culture²⁹. To investigate this in the context of a SARS-CoV-2-induced immune response, we collected animal sera at 14dpi and found that similarly high levels of antibody responses were triggered in vehicle and clofazimine groups, indicating that clofazimine did not induce significant suppression of humoral immune response of B lymphocyte (Extended Data Figure 5b). Furthermore, RNA-seq of hamster lung tissues was performed (Extended Data Figure 6a). Out of the 73 up-regulated genes after prophylactic clofazimine treatment (Supplementary Table 3), 34 (46.6%) were mapped to immune response related biological processes (Extended Data Figure 6b). Interestingly, within these 34 genes, 13 genes were mapped to "Leukocyte differentiation" GO category, including two major histocompatibility complex (MHC) class II molecules, H2-Aa and H2-Ab1 (labeled with * in Extended Data Figure 6c). In addition, transcription factors including Fos, Junb and Egr1 were also upregulated, which is consistent with the transcriptomic analysis on Caco-2 cells treated by clofazimine (Extended Data Figure 6c). Notably, most of the immune response-related genes were not changed after administering clofazimine to uninfected hamsters, indicating that clofazimine priming of the host response is dependent on SARS-CoV-2 infection, and may not result in undue activation of host immune system (Extended Data Figures 6d and 6e).

To determine the severity of lung damage, histological examination of hematoxylin and eosin (H&E) stained lung tissues was performed.

Control hamster lungs showed severe pathological changes, which were evidenced by large areas of consolidation as well as cell infiltrations in endothelium of blood vessel, and peribronchiolar regions. In contrast, clofazimine- or remdesivir-treated lung exhibited improved morphology and milder infiltrations (Extended Data Figure 7a and 7b). Taken together, clofazimine conferred protection against SARS-CoV-2 challenge by reducing the virus replication and the associated inflammatory dysregulation.

Antiviral synergy with remdesivir

Remdesivir is considered the current standard of care for the COVID-19 treatment. Intriguingly, we found that co-application of clofazimine and remdesivir impacts SARS-CoV-2 replication in a manner that extends beyond the additive activity predicted by the Bliss independence model (maximal Bliss Synergy Score of 44.28), which indicates that these two drugs harbor a synergistic antiviral relationship (Extended Data Figure 8a and 8b). Addition of 1.25 μ M clofazimine (4-fold EC_{50}) in an *in vitro* assay resulted in a nearly 20-fold decrease in concentrations of remdesivir required to inhibit viral replication by 90% (Extended Data Figure 8c). Importantly, the combination of drugs did not elicit additional cellular cytotoxicity (Extended Data Figure 8d).

To explore their antiviral synergy *in vivo* and to recapitulate the scenario that most COVID-19 patients will be treated after disease onset, SARS-CoV-2-infected hamsters were given oral clofazimine and intraperitoneal remdesivir together, with the first doses given 24h after virus challenge. Experimentally, 10-fold lower of remdesivir standard dosing, i.e. 1.5 mg/kg remdesivir and reduced clofazimine dosing, i.e. 15 mg/kg (corresponding to 100 mg/human) were given (Figure 4a). Significant improvement of weight loss was achieved in combinatorial group at 3dpi, either compared with the vehicle control or low-dose remdesivir group (Figure 4b). Monotherapy of low-dose remdesivir caused marginal reduction of lung virus titer. Additional application of clofazimine, however, not only exhibited potent synergy in terms of viral load (Figure 4c), but also restricted virus replication in the focal bronchiolar epithelial cells from spreading to alveolar areas (Extended Data Figure 9a). Importantly, the antiviral synergy suppressed virus shedding in the nasal wash (Figure 4d), which was not achievable with therapeutic remdesivir or clofazimine treatment individually (Figure 3e). The result is also evidenced by the immunofluorescence staining of hamster nasal turbinate with effectively diminished NP antigen expression as observed in the epithelium after the combinatorial treatment (Extended Data Figure 9b and 9c). Taken together, the antiviral synergy between low dose remdesivir and clofazimine significantly improved viral control, with reduced body weight loss, suppressed pulmonary virus titer, and nasal virus shedding, as well as decreased drug dosages.

Discussion

Clofazimine was first used to treat leprosy in 1969 and gained FDA approval in 1996³⁰. It is an orally bioavailable drug that is included in the WHO Model List of Essential Medicines. It is generally well-tolerated, and recommended as a WHO group C drug for treatment of multi-drug resistant tuberculosis (MDR-TB) and extensively drug-resistant tuberculosis (XDR-TB)³¹.

In SARS-CoV-2 infection, a delayed innate immune response may result in uncontrolled cytokine storm^{32,33}. Clofazimine's effect on rewiring the transcriptional landscape of the cell towards an antiviral status may be important in the disease setting, and understanding the contribution of this activity toward *in vivo* disease amelioration can provide insight towards its potential to improve viral control through enhancement of innate immune activities^{34,35}. Further elucidation of how clofazimine treatment may balance the regulation of innate and adaptive immune responses will be important to understand its potential clinical efficacy.

Online content

Any methods, additional references, Nature Research reporting summaries, source data, extended data, supplementary information, acknowledgements, peer review information; details of author contributions and competing interests; and statements of data and code availability are available at <https://doi.org/10.1038/s41586-021-03431-4>.

1. Peiris, J. S. *et al.* Coronavirus as a possible cause of severe acute respiratory syndrome. *Lancet* **361**, 1319–1325, [https://doi.org/10.1016/s0140-6736\(03\)13077-2](https://doi.org/10.1016/s0140-6736(03)13077-2) (2003).
2. Zaki, A. M., van Boheemen, S., Bestebroer, T. M., Osterhaus, A. D. & Fouchier, R. A. Isolation of a novel coronavirus from a man with pneumonia in Saudi Arabia. *N Engl J Med* **367**, 1814–1820, <https://doi.org/10.1056/NEJMoa1211721> (2012).
3. Barry, V. C. *et al.* A New Series of Phenazines (Rimino-Compounds) With High Antituberculosis Activity. *Nature* **179**, 1013–1015, <https://doi.org/10.1038/1791013a0> (1957).
4. Organization, W. H. *Coronavirus Disease (COVID-19) Situation Reports*, <<https://www.who.int/emergencies/diseases/novel-coronavirus-2019/situation-reports>> (2020).
5. Chan, J. F. *et al.* A familial cluster of pneumonia associated with the 2019 novel coronavirus indicating person-to-person transmission: a study of a family cluster. *Lancet* **395**, 514–523, [https://doi.org/10.1016/S0140-6736\(20\)30154-9](https://doi.org/10.1016/S0140-6736(20)30154-9) (2020).
6. Hung, I. F. *et al.* SARS-CoV-2 shedding and seroconversion among passengers quarantined after disembarking a cruise ship: a case series. *Lancet Infect Dis* **20**, 1051–1060, [https://doi.org/10.1016/S1473-3099\(20\)30364-9](https://doi.org/10.1016/S1473-3099(20)30364-9) (2020).
7. Chan, J. F., To, K. K., Tse, H., Jin, D. Y. & Yuen, K. Y. Interspecies transmission and emergence of novel viruses: lessons from bats and birds. *Trends Microbiol* **21**, 544–555, <https://doi.org/10.1016/j.tim.2013.05.005> (2013).
8. Chan, J. F. *et al.* Middle East respiratory syndrome coronavirus: another zoonotic betacoronavirus causing SARS-like disease. *Clin Microbiol Rev* **28**, 465–522, <https://doi.org/10.1128/CMR.00102-14> (2015).
9. Zumla, A., Chan, J. F., Azhar, E. I., Hui, D. S. & Yuen, K. Y. Coronaviruses - drug discovery and therapeutic options. *Nat Rev Drug Discov* **15**, 327–347, <https://doi.org/10.1038/nrd.2015.37> (2016).
10. Sheahan, T. P. *et al.* Broad-spectrum antiviral GS-5734 inhibits both epidemic and zoonotic coronaviruses. *Sci Transl Med* **9**, <https://doi.org/10.1126/scitranslmed.aal3653> (2017).
11. Beigel, J. H. *et al.* Remdesivir for the Treatment of Covid-19 - Preliminary Report. *N Engl J Med*, <https://doi.org/10.1056/NEJMoa2007764> (2020).
12. Wang, Y. *et al.* Remdesivir in adults with severe COVID-19: a randomised, double-blind, placebo-controlled, multicentre trial. *Lancet* **395**, 1569–1578, [https://doi.org/10.1016/S0140-6736\(20\)31022-9](https://doi.org/10.1016/S0140-6736(20)31022-9) (2020).
13. Goldman, J. D. *et al.* Remdesivir for 5 or 10 Days in Patients with Severe Covid-19. *N Engl J Med*, <https://doi.org/10.1056/NEJMoa2015301> (2020).
14. Hung, I. F. *et al.* Triple combination of interferon beta-1b, lopinavir-ritonavir, and ribavirin in the treatment of patients admitted to hospital with COVID-19: an open-label, randomised, phase 2 trial. *Lancet* **395**, 1695–1704, [https://doi.org/10.1016/S0140-6736\(20\)31042-4](https://doi.org/10.1016/S0140-6736(20)31042-4) (2020).
15. Riva, L. *et al.* Discovery of SARS-CoV-2 antiviral drugs through large-scale compound repurposing. *Nature*, <https://doi.org/10.1038/s41586-020-2577-1> (2020).
16. Gopal, M., Padayatchi, N., Metcalfe, J. Z. & O'Donnell, M. R. Systematic review of clofazimine for the treatment of drug-resistant tuberculosis. *Int J Tuberc Lung Dis* **17**, 1001–1007, <https://doi.org/10.5588/ijtld.12.0144> (2013).
17. Schaadlanyi, Z., Dieterle, W., Dubois, J. P., Theobald, W. & Vischer, W. Pharmacokinetics of Clofazimine in Healthy-Volunteers. *International Journal of Leprosy and Other Mycobacterial Diseases* **55**, 9–15 (1987).
18. Mansfield, R. E. Tissue Concentrations of Clofazimine (B663) in Man. *American Journal of Tropical Medicine and Hygiene* **23**, 1116–1119, <https://doi.org/10.4269/ajtmh.1974.23.1116> (1974).
19. Kissler, S. M., Tedijanto, C., Goldstein, E., Grad, Y. H. & Lipsitch, M. Projecting the transmission dynamics of SARS-CoV-2 through the postpandemic period. *Science* **368**, 860–868, <https://doi.org/10.1126/science.abb5793> (2020).
20. Sharma, A. *et al.* Human iPSC-Derived Cardiomyocytes Are Susceptible to SARS-CoV-2 Infection. *Cell reports. Medicine* **1**, 100052–100052, <https://doi.org/10.1016/j.xcr.2020.100052> (2020).
21. Yuan, S. *et al.* SREBP-dependent lipidomic reprogramming as a broad-spectrum antiviral target. *Nat Commun* **10**, 120, <https://doi.org/10.1038/s41467-018-08015-x> (2019).
22. Clausen, T. M. *et al.* SARS-CoV-2 Infection Depends on Cellular Heparan Sulfate and ACE2. *Cell* **183**, 1043, <https://doi.org/10.1016/j.cell.2020.09.033> (2020).
23. Lu, L. *et al.* Structure-based discovery of Middle East respiratory syndrome coronavirus fusion inhibitor. *Nat Commun* **5**, 3067, <https://doi.org/10.1038/ncomms4067> (2014).
24. Xia, S. *et al.* A pan-coronavirus fusion inhibitor targeting the HR1 domain of human coronavirus spike. *Sci Adv* **5**, eaav4580, <https://doi.org/10.1126/sciadv.aav4580> (2019).
25. Chen, J. *et al.* Structural Basis for Helicase-Polymerase Coupling in the SARS-CoV-2 Replication-Transcription Complex. *Cell* **182**, 1560–1573 e1513, <https://doi.org/10.1016/j.cell.2020.07.033> (2020).
26. Chan, J. F. *et al.* Simulation of the clinical and pathological manifestations of Coronavirus Disease 2019 (COVID-19) in golden Syrian hamster model: implications for disease pathogenesis and transmissibility. *Clin Infect Dis*, <https://doi.org/10.1093/cid/ciaa325> (2020).
27. Nix, D. E. *et al.* Pharmacokinetics and relative bioavailability of clofazimine in relation to food, orange juice and antacid. *Tuberculosis (Edinb)* **84**, 365–373, <https://doi.org/10.1016/j.tube.2004.04.001> (2004).
28. Herold, T. *et al.* Elevated levels of IL-6 and CRP predict the need for mechanical ventilation in COVID-19. *J Allergy Clin Immunol* **146**, 128–136 e124, <https://doi.org/10.1016/j.jaci.2020.05.008> (2020).
29. Cholo, M. C., Steel, H. C., Fourie, P. B., Germishuizen, W. A. & Anderson, R. Clofazimine: current status and future prospects. *J Antimicrob Chemother* **67**, 290–298, <https://doi.org/10.1093/jac/dkr444> (2012).
30. Hwang, T. J. *et al.* Safety and availability of clofazimine in the treatment of multidrug and extensively drug-resistant tuberculosis: analysis of published guidance and meta-analysis of cohort studies. *BMJ open* **4**, e004143–e004143, <https://doi.org/10.1136/bmjopen-2013-004143> (2014).
31. Falzon, D. *et al.* World Health Organization treatment guidelines for drug-resistant tuberculosis, 2016 update. *Eur Respir J* **49**, <https://doi.org/10.1183/13993003.02308-2016> (2017).
32. Hadjadj, J. *et al.* Impaired type I interferon activity and inflammatory responses in severe COVID-19 patients. *Science* **369**, 718–724, <https://doi.org/10.1126/science.abc6027> (2020).
33. Lucas, C. *et al.* Longitudinal analyses reveal immunological misfiring in severe COVID-19. *Nature* **584**, 463–469, <https://doi.org/10.1038/s41586-020-2588-y> (2020).
34. Swanson, R. V. *et al.* Pharmacokinetics and pharmacodynamics of clofazimine in a mouse model of tuberculosis. *Antimicrob Agents Chemother* **59**, 3042–3051, <https://doi.org/10.1128/AAC.00260-15> (2015).
35. <<https://www.gilead.com/news-and-press/press-room/press-releases/2020/6/an-open-letter-from-daniel-oday-chairman--ceo-gilead-sciences>> (2020).
36. Weng, Z. *et al.* A simple, cost-effective but highly efficient system for deriving ventricular cardiomyocytes from human pluripotent stem cells. *Stem Cells Dev* **23**, 1704–1716, <https://doi.org/10.1089/scd.2013.0509> (2014).
37. Chan, J. F. *et al.* Development and Evaluation of Novel Real-Time Reverse Transcription-PCR Assays with Locked Nucleic Acid Probes Targeting Leader Sequences of Human-Pathogenic Coronaviruses. *J Clin Microbiol* **53**, 2722–2726, <https://doi.org/10.1128/JCM.01224-15> (2015).
38. Chu, H. *et al.* Comparative replication and immune activation profiles of SARS-CoV-2 and SARS-CoV in human lungs: an ex vivo study with implications for the pathogenesis of COVID-19. *Clin Infect Dis*, <https://doi.org/10.1093/cid/ciaa410> (2020).
39. Yuan, S. *et al.* Metalloproteinase bismuth citrate suppresses SARS-CoV-2 replication and relieves virus-associated pneumonia in Syrian hamsters. *Nat Microbiol* **5**, 1439–1448, <https://doi.org/10.1038/s41564-020-00802-x> (2020).
40. Kim, D. *et al.* TopHat2: accurate alignment of transcriptomes in the presence of insertions, deletions and gene fusions. *Genome Biol* **14**, R36, <https://doi.org/10.1186/gb-2013-14-4-r36> (2013).
41. Liao, Y., Smyth, G. K. & Shi, W. featureCounts: an efficient general purpose program for assigning sequence reads to genomic features. *Bioinformatics* **30**, 923–930, <https://doi.org/10.1093/bioinformatics/btt656> (2014).
42. Yu, G., Wang, L. G., Han, Y. & He, Q. Y. clusterProfiler: an R package for comparing biological themes among gene clusters. *OMICS* **16**, 284–287, <https://doi.org/10.1089/omi.2011.0118> (2012).
43. Zhou, Y. Y. *et al.* Metascape provides a biologist-oriented resource for the analysis of systems-level datasets. *Nature Communications* **10**, <https://doi.org/10.1038/s41467-019-09234-6> (2019).
44. Hoffmann, M. *et al.* SARS-CoV-2 Cell Entry Depends on ACE2 and TMPRSS2 and Is Blocked by a Clinically Proven Protease Inhibitor. *Cell* **181**, 271–280.e278, <https://doi.org/10.1016/j.cell.2020.02.052> (2020).
45. Xie, X. *et al.* An Infectious cDNA Clone of SARS-CoV-2. *Cell Host & Microbe* **27**, 841–848.e843, <https://doi.org/10.1016/j.chom.2020.04.004> (2020).

Publisher's note Springer Nature remains neutral with regard to jurisdictional claims in published maps and institutional affiliations.

© The Author(s), under exclusive licence to Springer Nature Limited 2021

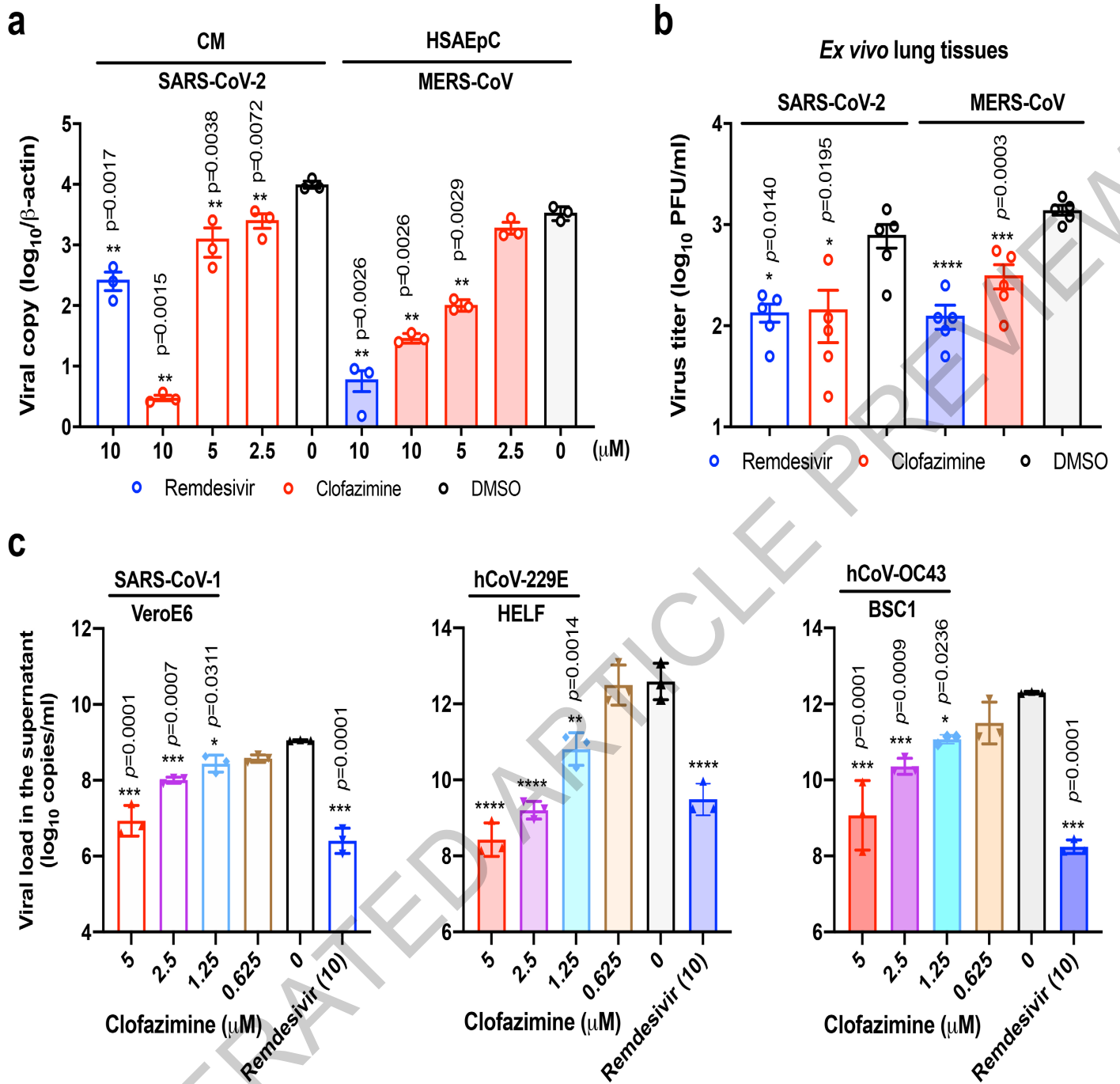


Fig. 1 | Clofazimine inhibits a broad-spectrum of human-pathogenic CoVs replication in human cellular models. (a) Clofazimine inhibited SARS-CoV-2 (0.1 MOI) replication in human primary CMs and MERS-CoV (1 MOI) replication in human primary HSAEpCs. Cell lysates were collected for viral load determination. Data represent mean \pm SD for n=3 biological replicates. Two-tailed student's t-test. (b) *Ex vivo* human lung tissues were infected with SARS-CoV-2 or MERS-CoV followed by clofazimine (10 μ M) or remdesivir (10 μ M) or DMSO (0.1%) treatment. Supernatants were collected for quantification of viral titer by plaque assay. Data represent mean \pm SD for n=5

biological replicates. Two-tailed student's t-test. (c) Antiviral activity of clofazimine against SARS-CoV (0.01 MOI, 48 hpi), hCoV-229E (0.001 MOI, 72 hpi), and hCoV-OC43 (0.001 MOI, 72 hpi) in cell lines as indicated. Viral load in the cell culture supernatant was quantified by RT-qPCR assays. Data represent mean \pm SD for n=3 biological replicates. One-way ANOVA followed by Sidak's post-test. All experiments were repeated twice for confirmation. All statistical analysis were compared with the DMSO group (0 μ M), ****p<0.0001, ***p<0.001, **p<0.01 and *p<0.05.

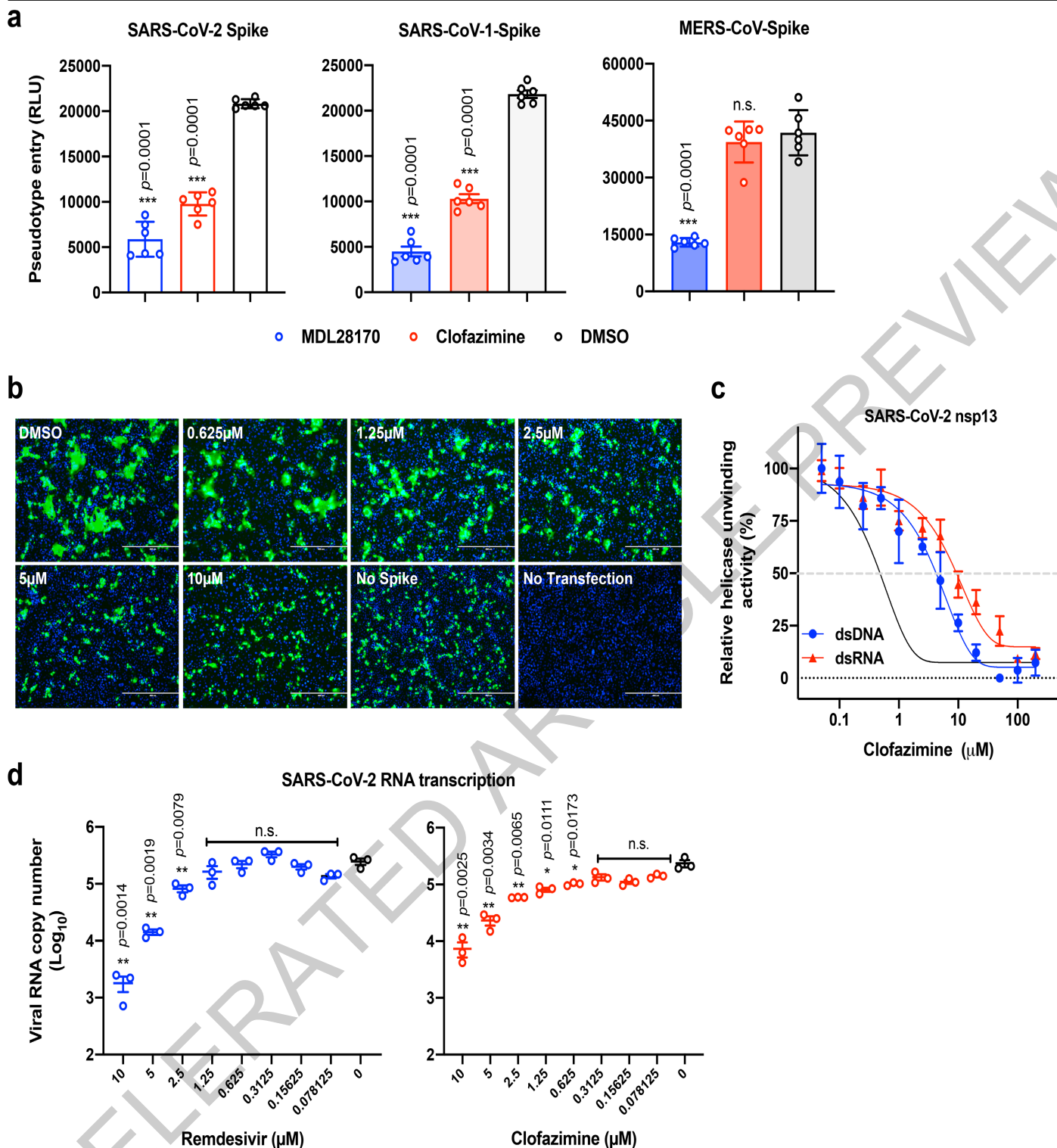


Fig. 2 | Clofazimine interferes with multiple steps of virus life cycle. (a) VSV-based pseudotyped viral particle assay. VeroE6 cells pre-treated with indicated compounds were infected with the indicated spike-pseudotyped particles. Luciferase signals were quantified at 24hpi. Shown are mean \pm SEM for $n=6$ independent experiments. One-way ANOVA followed by Dunnett post-test. MDL28170 was utilized as a positive control CoV entry inhibitor¹⁵. **(b)** Clofazimine inhibits SARS-CoV-2 spike-mediated membrane fusion. Vero cells co-transfected with SARS-CoV-2-spike and EGFP plasmids were added to the non-transfected Vero cells to induce membrane fusion. Confocal images were acquired at 48 h post-transfection. Scale bar: 400 μ m. Shown are representative images each selected from a pool of images captured in two independent experiments. **(c)** *In vitro* transcribed viral RNA replication assay.

Remdesivir (blue circles) or clofazimine (red circles) were added at the indicated doses. Negative-stranded RNA was then quantified at 12h post-electroporation. Error bars represent SEM for $n=3$ independent experiments. Two-tailed student's t-test. **(d)** Titration of the DNA- and RNA-unwinding activity of the SARS-CoV-2 helicase by clofazimine using a FRET-based assay. The black curve represents a positive control inhibitor (ranitidine bismuth citrate) using DNA-based substrate. Data represent mean \pm SD for $n=3$ biological replicates. The experiments were repeated twice for confirmation. All statistical analysis were compared with the DMSO or non-treatment group, **** $p < 0.0001$, *** $p < 0.001$, ** $p < 0.01$, * $p < 0.05$, and n.s. indicates $p > 0.05$.

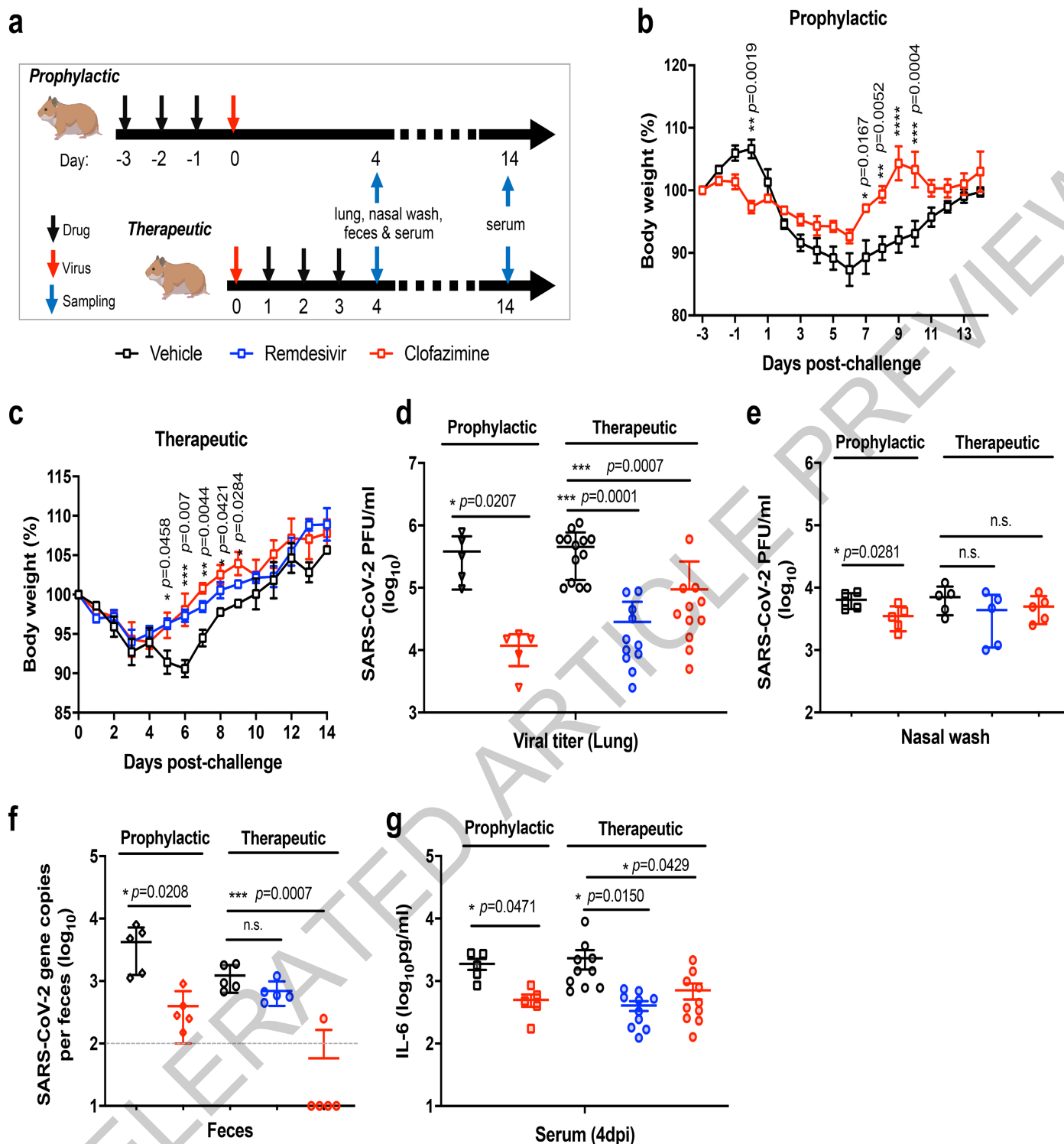


Fig. 3 | Prophylactic and therapeutic treatment with clofazimine reduces SARS-CoV-2 disease. (a) Prophylactic treatment used oral administration of clofazimine given at -3, -2 and -1dpi, followed by virus challenge at 0dpi; therapeutic administration of clofazimine was performed at 1, 2, and 3dpi. Tissue samples were collected at indicated days post-infection. Remdesivir (blue symbols) was included as a control in the therapeutic regimen. (b and c) Daily body weights of the animals under prophylactic (b) or therapeutic (c) treatment. Data is shown as mean \pm SEM of $n=3$ animals/group. Two-way ANOVA followed by Sidak's post-test for prophylactic groups and two-way ANOVA followed by Tukey's post-test for therapeutic groups. P value indicates clofazimine vs vehicle groups. (d) Viral yield in the hamster lung tissue, after prophylactic ($n=5$ animals/group) or therapeutic treatment ($n=11$ animals for each remdesivir and clofazimine group and $n=13$ animals for vehicle group),

were harvested at 4 dpi and titrated by plaque assays. (e) Hamster nasal washes collected on 4 dpi were subjected to live virus titration by plaque assays ($n=5$ animals/group). (f) Hamster feces freshly collected at 4 dpi were subjected to SARS-CoV-2 viral copy detection by RT-qPCR assays ($n=5$ animals/group). For statistical analysis purpose, a value of 10-100 was assigned for any data point below the detection limit (the dotted line). (g) IL-6 level in hamster serum was quantified. $n=5$ animals for each prophylaxis group and $n=10$ animals for each therapeutic group. All data from (d-g) are shown as mean \pm SD. Two-tailed student's t-test for prophylaxis groups and one-way ANOVA followed by Dunnett's post-test for therapeutic groups comparing with the vehicle group (black symbols). **** $p<0.0001$, *** $p<0.001$, ** $p<0.01$, * $p<0.05$, and n.s. indicates $p>0.05$.

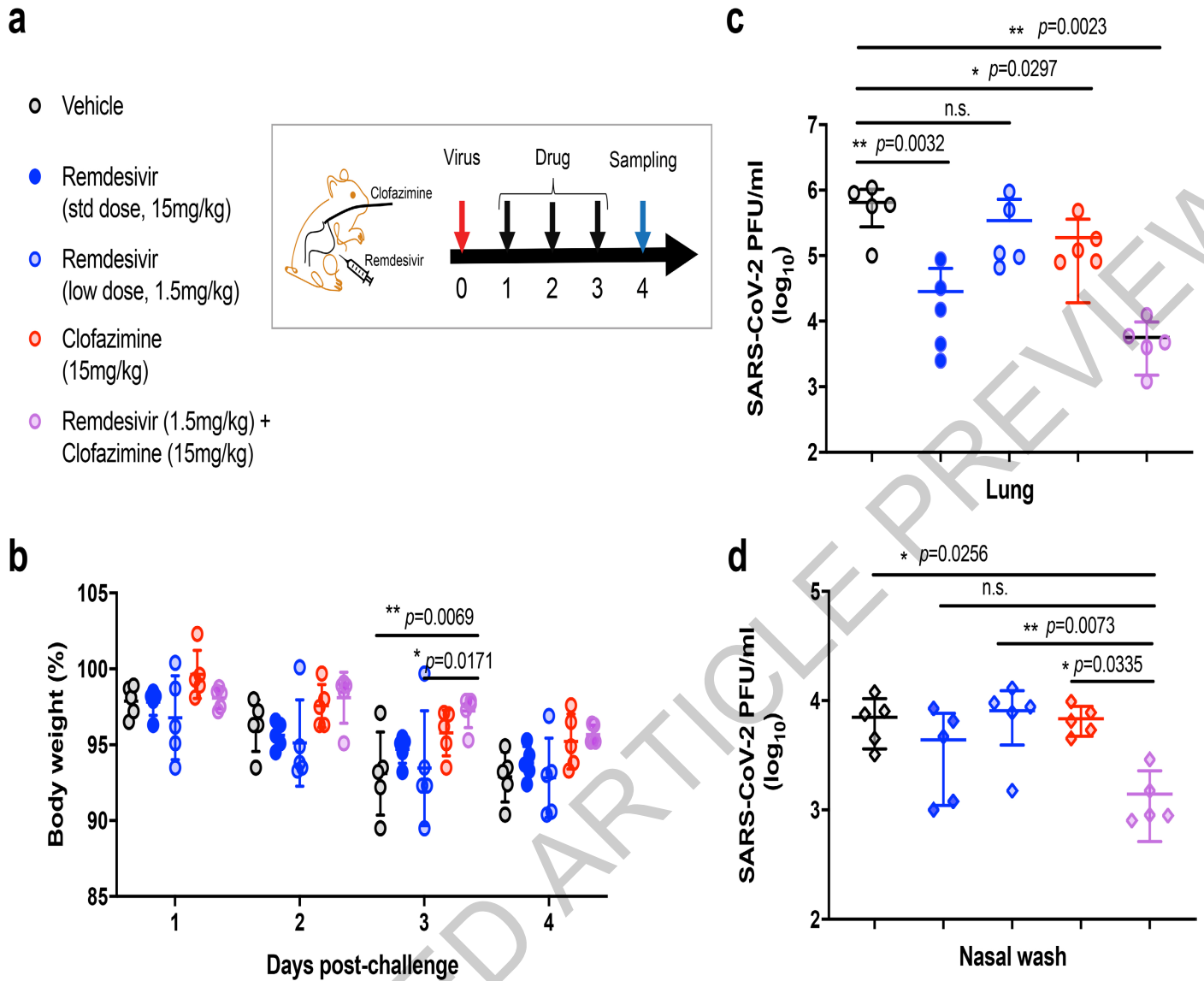


Fig. 4 | Clofazimine exhibits antiviral synergy with remdesivir in hamsters. (a) Experimental design of *in vivo* study: oral clofazimine and/or intraperitoneal remdesivir were administered at indicated dpi. Vehicle control hamsters received oral administration of corn oil and intraperitoneal injection of 2% DMSO in 12% SBE- β -CD. (b) Daily body weights of the hamsters (n=5 animals/group). Data are shown as mean \pm SD by two-way ANOVA followed

by Tukey's test. (c) Virus in the hamster lung tissue was titrated by plaque assay. One-way ANOVA followed by Dunnett post-test (n=5 animals/group). (d) Virus titer in the nasal wash was determined by plaque assays. One-way ANOVA followed by Dunnett post-test and compared with the combinatorial group (n=5 animals/group). For all statistical analysis, **p<0.01, *p<0.05 and n.s. indicates non-significant.

Materials and methods

Cells and viruses

Different cell lines and primary cells were utilized which are their highly sensitivity to each CoV replication, correspondingly. Human hepatoma Huh7 (JCRB, 0403) cells, human colon Caco-2 cells (ATCC, HTB-37), monkey Vero E6 cells (ATCC, CRL-1586), monkey kidney BSC-1 cells (ATCC, CCL-26) were maintained in DMEM culture medium supplemented with 10% heat-inactivated FBS, 50 U/mL penicillin and 50 µg/mL streptomycin. Human embryonic lung fibroblasts (HELFL) were developed in house. Human primary small airway epithelial cells (HSAEpC, ATCC, PCS-301-010) were cultured with airway epithelial cell basal medium according to the manufacturer's protocol. Ventricular cardiomyocytes (CMs) were differentiated from the human embryonic stem cell HES2 (ESI) maintained in mTeSR1 medium (STEMCELL Technologies)³⁶. Briefly, HES2 cells were dissociated with Accutase (Invitrogen) into single cells suspensions on day 0. Cells were seeded on low-attachment culture vessels (Corning) and cultured in mTeSR1 medium supplemented with 40 µg/mL Matrigel, 1 ng/mL BMP4 (Invitrogen) and 10 µM Rho kinase inhibitor (ROCK) (R&D) under hypoxic environment with 5% O₂. From day 1 to 3, cells were cultured in Stem-Pro34 SFM (Invitrogen) with 50 µg/mL ascorbic acid (AA) (Sigma), 2 mM Gluta-MAX (Invitrogen), 10 ng/mL BMP4, and 10 ng/mL human recombinant activin-A (Invitrogen). From day 4 to day 7, 5 µM Wnt inhibitor IWR-1 (Tocris) was added. From day 8 to day 14, cells were cultured under normoxia in RPMI 1640 medium (Invitrogen) supplemented with 2 mM Gluta-MAX, 1×B-27 supplement (Invitrogen) and 50 µg/mL AA. The cells were then dissociated with Accutase and seeded as monolayer in desired culture vessels for 3 days before infections. The SARS-CoV-2 HKU-001a strain (GenBank accession number: MT230904) was isolated from the nasopharyngeal aspirate specimen of a laboratory-confirmed COVID-19 patient in Hong Kong²⁶. The SARS-CoV-2 Isolate USA-WA1/2020 was deposited by the Centers for Disease Control and Prevention and obtained through BEI Resources. The MERS-CoV (HCoV-EMC/2012) was a gift from Dr. Ron Fouchier. Archived clinical strains of SARS-CoV-1, HCoV-OC43, and HCoV-229E were obtained from the Department of Microbiology, The University of Hong Kong (HKU)³⁷. All experiments involving live SARS-CoV-1, SARS-CoV-2 and MERS-CoV followed the approved standard operating procedures of the Biosafety Level 3 facility at the University of Hong Kong and Sanford Burnham Prebys Medical Discovery Institute as we previously described.

Antiviral evaluation in human *ex vivo* lung tissues

Human lung tissues for *ex vivo* studies were obtained from patients undergoing surgical operations at Queen Mary Hospital, Hong Kong as previously described³⁸. The donors and/or parents of the donor gave written consent as approved by the Institutional Review Board of the University of Hong Kong/Hospital Authority Hong Kong West Cluster (UW13-364). The freshly obtained lung tissues were processed into small rectangular pieces and were rinsed with advanced DMEM/F12 medium (Gibco) supplemented with 2 mM of HEPES (Gibco), 1×GlutaMAX (Gibco), 100 U/mL penicillin, and 100 µg/mL streptomycin. The specimens were infected with SARS-CoV-2 HKU-001a or MERS-CoV with an inoculum of 1×10⁶ PFU/mL at 500 µL per well. After two hours, the inoculum was removed, and the specimens were washed 3 times with PBS. The infected human lung tissues were then cultured in 1 mL of advanced DMEM/F12 medium with 2 mM HEPES (Gibco), 1×GlutaMAX (Gibco), 100 U/mL penicillin, 100 µg/mL streptomycin, 20 µg/mL vancomycin, 20 µg/mL ciprofloxacin, 50 µg/mL amikacin, and 50 µg/mL nystatin. Supernatants were collected at 24 hours post inoculation (hpi) for plaque assays.

Antiviral assessment in a SARS-CoV-2 infected hamster model

Male and female Syrian hamster, aged 6-10 weeks old, were obtained from the Chinese University of Hong Kong Laboratory Animal Service

Centre through the HKU Centre for Comparative Medicine Research. The hamsters were kept in biosafety level 2 housing and given access to standard pellet feed and water ad libitum as we previously described²⁶. All experimental protocols were approved by the Animal Ethics Committee in the University of Hong Kong (CULATR) and were performed according to the standard operating procedures of the biosafety level 3 animal facilities (Reference code: CULATR 5370-20). Experimentally, each hamster was intranasally inoculated with 10⁵ PFU of SARS-CoV-2 in 100 µL PBS under intraperitoneal ketamine (200 mg/kg) and xylazine (10 mg/kg) anesthesia.

To simulate the prescribed human dosage (200 mg QD), an equivalent hamster dose of 25 mg/kg/day was converted based on body surface area. Specifically, 25 mg/kg (hamster) × 0.13 (conversion factor) = 3.25 mg/kg (Human equivalent dose), and a 60 kg human requires 3.25 mg/kg × 60 kg = 195 mg clofazimine per day. Prophylactic treatment used oral administration of clofazimine given on -3, -2 and -1dpi (25 mg/kg), followed by virus challenge at 0dpi, while therapeutic post-exposure and oral administration of clofazimine (Sigma-Aldrich, C8895) were performed on 1, 2, and 3 dpi (25 mg/kg) with the first dosage given at 24 hpi. Clofazimine was delivered using corn oil (Sigma-Aldrich, C8267) as vehicle. Remdesivir was included as a positive control drug and dosed at 15 mg/kg via intraperitoneal route based on its effective dosage in SARS-CoV-infected mice¹⁰. Remdesivir (15 mg/kg, MedChemExpress) was prepared as 100 mg/ml stock in DMSO and further diluted using 12% SBE-β-CD before intraperitoneal injection. Hamsters receiving pure corn oil (oral) and 2% DMSO in 12% SBE-β-CD (intraperitoneal) was utilized as the vehicle control group. Animals were sacrificed at 4 dpi for virological and histopathological analyses. Viral yield in the lung tissue homogenates and/or feces were detected by plaque assay and/or RT-qPCR methods. Nasal washes were collected to exam virus shedding via respiratory tract. Hamsters were treated with isoflurane lightly, after that, 200 µL of PBS was injected into one nasal opening while collecting the turbid wash from the other one without any blood contamination. The nasal wash was filtered through 0.22 µm before subjecting to plaque assay. ELISA kit was utilized to determine the Interleukin 6 (IL-6) amount in the hamster sera on 4 dpi according to the manufacture's recommendations (ELISAGenie, HMF10001). Tissue pathology of infected animals was examined by H&E staining in accordance to the established protocol³⁹. On 14 dpi, enzyme immunoassay (EIA) was utilized to determine the antibody titer of hamster sera against SARS-CoV-2 NP antigen. Briefly, 96-well immune-plates (Nunc) were coated with 100 µL/well (0.1 µg/well) of SARS-CoV-2 NP in 0.05 M NaHCO₃ (pH 9.6) overnight at 4 °C. After blocking, 100 µL of heat-inactivated serum samples were serial-diluted before adding to the wells and incubated at 37 °C for 1 h. The attached antibodies were detected using horseradish-peroxidase-conjugated rabbit anti-hamster IgG antibody (Thermo Fisher Scientific; A18895; 1:2000). The reaction was developed by adding diluted 3,3',5,5'-tetramethylbenzidine single solution (TMB, Invitrogen) and stopped with 0.3 N H₂SO₄. The optical density (OD) was read at 450/620 nm using a microplate reader.

RNA-Seq analysis

Fastq files from RNA-seq were quality examined by FastQC (v0.11.7) (<https://www.bioinformatics.babraham.ac.uk/projects/fastqc/>). Reads were processed by cutadapt to remove reads with low quality and to trim adapters. For RNA-seq on Caco-2 cells, trimmed reads were aligned to hg38 reference genome and NCBI SARS-CoV-2 reference genome (NC_045512.2) using TopHat⁴⁰(v2.1.1); and for RNA-seq data from hamster lung tissues were mapped to MesAur1.0 (GCA_000349665.1) downloaded from Ensembl. Reads assigned to each gene were counted by featureCounts⁴¹ (v2.0.1) with human refseq gene sets as references for Caco-2 cells, and gene annotation of golden hamster from Ensembl database for hamster dataset, respectively. Genes without at least 1 read mapped on average in each sample were considered undetectable and were filtered out. Read counts were normalized by Trimmed Mean of

Article

M-values (TMM) method and differential expression was calculated using R package edgeR (v3.28.1) and Genewise Negative Binomial Generalized Linear Models with Quasi-likelihood Tests (glmQLFit) method was used for statistical tests. Cut-offs imposed for differential expression analysis was set as False Discovery Rate (FDR) of 0.05 and fold change >2 or <0.5. The pathway analysis was performed by R package clusterProfiler⁴² (v3.14.3) and Metascape⁴³. Heatmaps were plotted using R package pheatmap (v1.0.12) (Kolde, R. (2013). pheatmap: Pretty Heatmaps. R package version 0.7.7. <http://CRAN.R-project.org/package=pheatmap>). Other plots were generated by R package ggplot2 (v3.3.0) (Wickham H (2016). ggplot2: Elegant Graphics for Data Analysis. Springer-Verlag New York. ISBN 978-3-319-24277-4, <https://ggplot2.tidyverse.org>). PCA analysis was performed by R package factoextra (1.0.7).

Pseudotyping of VSV and Pseudotype-based inhibition assay

Vesicular Stomatitis Virus (VSV) pseudotyped with spike proteins of MERS-CoV, SARS-CoV-1, and SARS-CoV-2 were generated as previously reported with some modifications⁴⁴. Briefly, BHK-21/WI-2 cells (Kerafast, MA) overexpressing the spike proteins were inoculated with VSV-G pseudotyped Δ G-luciferase VSV (Kerafast, MA). After 2 h inoculation at 37 °C, the inoculum was removed and cells were re-fed with DMEM supplemented with 5% FBS and VSV-G antibody (1I, mouse hybridoma supernatant from CRL-2700; ATCC; 1:100). Pseudotyped particles were collected at 24 h post-inoculation, then centrifuged at 1,320 × g to remove cell debris and stored at -80 °C until use.

To determine the effect of the compounds on viral entry, Vero E6 cells were treated with clofazimine at a concentration of 2.5 μ M for 1 h prior to inoculation with respective pseudotyped VSV. After 2 h inoculation in the presence of the compounds, the inoculum was removed and cells were re-fed with fresh medium for further culture. The activity of firefly luciferase was measured using bright-Glo™ luciferase assay (Promega) for quantitative determination at 16 h post-transduction.

The effect of clofazimine on SARS-CoV-2 viral replication

The full-length SARS-CoV-2 viral RNA transcripts were *in vitro* synthesized from an infectious clone of SARS-CoV-2 (kindly provided by Pei-Yong Shi, UTMB) according to a recently published protocol⁴⁵. 10 μ g of total RNA transcripts and 5 μ g SARS-CoV-2 NP gene transcript were mixed with Vero E6 cells stably expressing SARS-CoV-2 NP protein and then added into a 0.2 cm cuvette for nucleofection with the 4D-Nucleofector™ Core Unit (Lonza) using pulse code V-001. Immediately after electroporation, 1000 μ L of pre-warmed media was added to the cuvette and cells were subsequently aliquoted into 384-well plates. Two hours post-seeding, compounds at different concentrations were added into each well. At 12 hours post-electroporation, intracellular and viral RNA was purified from the treated cells with TurboCapture 384 mRNA Kit (Qiagen) in accordance with the manufacturer's instructions. The purified RNA was subjected to first-strand cDNA synthesis using the high-capacity cDNA reverse transcription kit (Applied Biosystems, Inc) with the following primer (TagRdRp-F: 5'-CGGTCATGGTGGCGAATAACCCTGTGGGTTTTACTTAA-3'). Real-time PCR analysis was performed using TaqPath 1-step RT-qPCR Master Mix (Applied Biosystems, Inc). The following primers and probe were used for negative-stranded RNA detection: Tag-F: 5'-CGGTCATGGTGGCGAATAACCCTGT-3'; ORF1ab-R: 5'-ACGATTGTGCATCAGCTGA-3'; ORF1ab-P: 5'-6FAM-CCGTCTGCGGTATGTGGAAGGTTATGG-BHQ1-3'). In parallel, 5 μ g of the *in vitro* transcribed GFP mRNA (StemMACS eGFP mRNA, Cat# 130-101-114) were electroporated into Vero E6 cells. At 2 h after seeding, cells were treated either with clofazimine or remdesivir, and then cultured for further 24 hours. The GFP signal was measured by flow cytometry analysis FlowJo (v10.0.7).

Detection of spike protein binding against ACE2 or heparin

Binding between the purified SARS-CoV-2 spike protein to the cellular entry factors ACE2 and heparin were detected by ELISA as we

previously described²². High binding microtiter plates were coated with heparin-BSA (100 ng/well) or recombinant ACE2 (200 ng/well) overnight at 4 °C. The plates were then blocked for 3 hr at 37 °C with TSM buffer (20 mM Tris buffer, pH 7.4, containing 150 mM NaCl, 2 mM MgCl₂, 2 mM CaCl₂, 0.05% Tween-20, and 1% BSA). Next, 10 nM biotinylated SARS-CoV-2 Spike protein in a dilution of clofazimine (10-0.1 μ M) in TSM buffer was added to the plates in triplicate. Bound biotinylated protein was detected by adding Avidin-HRP (405103, BioLegend) diluted 1:2000 in TSM buffer. Lastly, the plates were developed with TMB turbo substrate for 5-15 min. The reaction was quenched using 1 M sulfuric acid and the absorbance was measured at 450 nm.

Spike-mediated membrane fusion assay

SARS-CoV-2 spike-mediated cell-cell fusion assay was performed as we previously established with some modifications²². Vero cells were co-transfected with 1 μ g SARS-CoV-2 spike plasmid and 0.4 μ g EGFP plasmid for 8 hours. In another 24-well plate, Vero cells (i.e. target cells expressing ACE2) were washed with PBS before co-cultured with the effector cells (i.e. Vero cells co-transfected with spike and EGFP), in the presence of indicated concentration of clofazimine. After another 48 h, spike-mediated membrane fusion, as reflected by the green fluorescence area, was evaluated using confocal imaging. Vero/EGFP cells without spike transfection was included as the negative control.

Time-of-addition assay

Time-of-drug-addition assay was performed to investigate which stage of SARS-CoV-2 life cycle clofazimine interfered with as previously described¹⁵. Briefly, Vero E6 cells were seeded in 96-well plates (4 × 10⁴ cells/well). The cells were infected by SARS-CoV-2 USA-WA1/2020 at an MOI of 1.5 and then incubated for additional 1 h. The viral inoculum was then removed, and the cells were washed twice with PBS. At 1 hpi (i.e., post entry), clofazimine at a concentration of 5 μ M was added to the infected cells at time-points indicated, followed by the incubation at 37 °C in 5% CO₂ until 10 hpi (i.e. one virus life cycle). Cells were fixed at 10 hpi for quantification of the percentage of infected cells using an immunofluorescence assay targeting SARS-CoV-2 NP.

In vitro primer elongation assay using RdRp core complex

Expression plasmids for SARS-CoV-2 nsp7, nsp8 and nsp12 were kindly provided by Seth Darst and Elizabeth Campbell lab. Expression and purification of nsp7/nsp8 and nsp12 were performed as described²⁵. Transcription scaffold was prepared by annealing 2:1:3 molar ratio of template strand RNA (5'-CUAUCCCCAUGUGAUUUU AAUAGCUUCUUAGGAGAAUGACGU AGCAUGCUACGG), 32^p labeled primer RNA (5'-CGCGUAGCAUGCUACGUCA UUCUCCUAGAAGCA) and non-template DNA (5'-ATCACATGGGGATAG) at 95 °C for 5 min and slow cool down to room temperature in elongation buffer (20 mM Tris pH 7.5, 40 mM KCl, 5 mM MgCl₂, 5 mM DTT). Prepared scaffold was incubated with different concentrations of clofazimine or SL-11128 for 2 hours at room temperature. SL-11128 was reported to be anti-SARS-CoV-2 effective in our previous report¹⁵. RdRp core complex was prepared by mixing 1:3 molar ratio of nsp12 and nsp7/8 and incubating for 20 min in ice. Scaffold was added to RdRp complex and incubated for 20 min at 30 °C. To start reaction, equal volume of rNTP was added to RdRp – scaffold complex. Final concentrations for assays were: 20 nM scaffold, 250 nM RdRp, 5-40 μ M of clofazimine or SL-11128, 10 μ M rNTPs. Reaction was quenched by mixing with loading buffer (90% formamide, 50 mM EDTA, 0.05% xylene cyanol and 0.05% bromophenol blue) at different time-points. All samples were denatured at 95 °C for 20 min and analyzed by 8% TBE/urea denaturing PAGE.

In vitro helicase unwinding assay using nsp13 protein

Helicase inhibition assays were performed as we previously described³⁹. The recombinant SARS-CoV-2 Nsp13 proteins were expressed in *E. coli* BL21(DE3) cells and purified using the Ni²⁺-loaded HiTrap Chelating

System (GE Healthcare) according to the manufacturer's instructions. The DNA oligomers FL-Cy3 oligo (5'-TTTTTTTTTTTTTTTTTTTTCGA GCACCGCTGCGGCTGCACC(Cy3)-3') and RL-BHQ oligo (5'-(BHQ2)GGT CAGCCG CAGC GGTGCTCG-3') were purchased from Metabion GmbH. RNA oligos including RNA_31/18-mer-Cy3 (5'-CGCAGUCUUCUCCUG GUGUCUGAACAGUGAC(Cy3)-3') and RNA_31/18-mer_BHQ (5'-(BHQ2) GUCACUGUUCGAGACCA-3') were synthesized from IDT. Both oligos were annealed in the buffer of 20 mM Tris-HCl pH 8.0 and 150 mM NaCl. Assays were performed in buffer composed of 20 mM Tris-HCl buffer, pH 7.4, 150 mM NaCl, 0.1 mg/mL BSA, 5 mM MgCl₂, 5 mM TCEP, 5% glycerol and 10 nM helicase, followed by addition of 0.5 μl of 100 mM ATP and 1.5 μl of oligo mixture to make the final concentration of FL-Cy3:RL BHQ oligo and RL oligo at 5 nM and 10 nM, respectively. Fluorescence (λ_{ex}=550 nm, λ_{em}=620 nm) was measured using SpectraMax® iD3 Multi-Mode microplate reader to determine the extent of DNA/RNA duplex unwinding.

Illustrations

Hamster illustrations in Figure 3a and Extended Data Figure 6a were created with BioRender software (<https://biorender.com/>).

Reporting summary

Further information on research design is available in the Nature Research Reporting Summary linked to this paper.

Data availability

Complete sequences of SARS-CoV-2 HKU-001a and SARS-CoV-2 USA-WA1/2020 are available through GenBank (accession numbers MT230904 (HKU-001a), MT246667 and MN908947 (USA-WA1/2020)). The raw RNA-Seq data discussed in this publication have been deposited in NCBI's Gene Expression Omnibus and are accessible through GEO Series accession number GSE162899. The hg38 reference genome is downloaded from UCSC database (<https://hgdownload.soe.ucsc.edu/goldenPath/hg38/bigZips/>). Refseq gene annotation is retrieved from UCSC Table Browser (<https://genome.ucsc.edu/cgi-bin/hgTables>). The NCBI SARS-CoV-2 reference genome (NC_045512.2) is downloaded from NCBI database (<https://www.ncbi.nlm.nih.gov/nucleotide/1798174254>). The MesAur1.0 genome assembly (GCA_000349665.1) and annotation are from Ensembl database (https://asia.ensembl.org/Mesocricetus_auratus/Info/Index). Other supporting raw data are available from the corresponding author upon reasonable request. Source data are provided with this paper.

46. Ianevski, A., Giri, A. K. & Aittokallio, T. SynergyFinder 2.0: visual analytics of multi-drug combination synergies. *Nucleic Acids Research* **48**, W488-W493, <https://doi.org/10.1093/nar/gkaa216> (2020).

Acknowledgements The authors acknowledge the assistance of the University of Hong Kong Li Ka Shing Faculty of Medicine Centre for PanorOmic Sciences. We thank Seth Darst and Elizabeth Campbell for providing us plasmids of nsp7/8 and nsp12, and Kamil Godula and Ryan Porell (University of California, San Diego) for heparin-BSA conjugate. This study was partly supported by funding to University of Hong Kong: the Health and Medical Research Fund (grant no. COVID190121 and CID-HKU11-11), the Food and Health Bureau, The Government of the Hong Kong Special Administrative Region; Sanming Project of Medicine in Shenzhen, China (SZSM201911014); and the High Level-Hospital Program, Health Commission of Guangdong Province, China; and donations from Richard Yu and Carol Yu, Shaw Foundation Hong Kong, Michael Seak-Kan Tong, May Tam Mak Mei Yip, Lee Wan Keung Charity Foundation Limited, Hong Kong Sanatorium & Hospital, Hui Ming, Hui Hoy and Chow Sin Lan Charity Fund Limited, Chan Yin Chuen Memorial Charitable Foundation, Marina Man-Wai Lee, the Hong Kong Hainan Commercial Association South China Microbiology Research Fund, the Jessie & George Ho Charitable Foundation, Perfect Shape Medical Limited, Kai Chong Tong, Norman & Cecilia Yip Foundation, Tse Kam Ming Laurence, Foo Oi Foundation Limited, Betty Hing-Chu Lee, Ping Cham So, and Lo Ying Shek Chi Wai Foundation. This work was also supported by the grants to the Sanford Burnham Prebys Medical Discovery Institute: DoD: W81XWH-20-1-0270; DHIPC: U19 AI118610; NCI Cancer Center grant P30 CA030199-40; Fluomics/NOSI: U19 AI135972, as well as generous philanthropic donations from Dinah Ruch and Susan & James Blair. The funding sources had no role in the study design, data collection, analysis, interpretation, or writing of the report.

Author contributions S.Y., X.Y., X.M., Z.W.Y., L.R., N.M., L.P., Y.P., R.L., C.C.Y.C., P.M.L., J.C., R.L., Y.Y.Z., Y.D.T. and W.X. designed and/or performed experiments. S.Y., X.Y., X.M., Z.W.Y., J.F.W.C., L.P., Y.D., K.H.S., and H.C. analyzed data. S.Y., X.Y., Z.W.Y., C.K.Y., K.H.K., K.Y.S., W.K.A., R.W., Y.Y.Z., Y.D.T., C.Y.L., T.M.C., J.P., J.O., and L.S. generated critical reagents. K.Y.Y., S.K.C., R.S., S.Y., X.Y., X.M., and L.P. wrote the manuscript. S.Y., J.F.W.C., C.C.S.C., V.K.M.P. and K.T. provided the animal data. A.C.Y.L., A.J.Z., S.Y., and J.F.W.C. performed histopathological evaluation. S.K.C., R.S., I.F.N.H., R.A.L., H.C., H.S., D.W., X.H.C., J.D.E., and D.Y.J. provided conceptual advice and troubleshooting. K.Y.Y., S.K.C., and R.S. oversaw the conception and supervised the study. K.Y.Y. and S.K.C. provided the grant support.

Competing interests J.F.W.C. has received travel grants from Pfizer Corporation Hong Kong and Astellas Pharma Hong Kong Corporation Limited and was an invited speaker for Gilead Sciences Hong Kong Limited and Luminex Corporation. S.K.C. are inventors on a patent application on repurposed antiviral compounds for SARS-CoV-2 owned by Scripps Research and Sanford Burnham Prebys. US Patent Application Serial No. 63/010630, entitled Methods and Compositions for Antiviral Treatment relates to aspects of this work and was filed on 15 April 2020. The corresponding authors had full access to all the data in the study and had final responsibility for the decision to submit for publication. The other authors declare no competing interests.

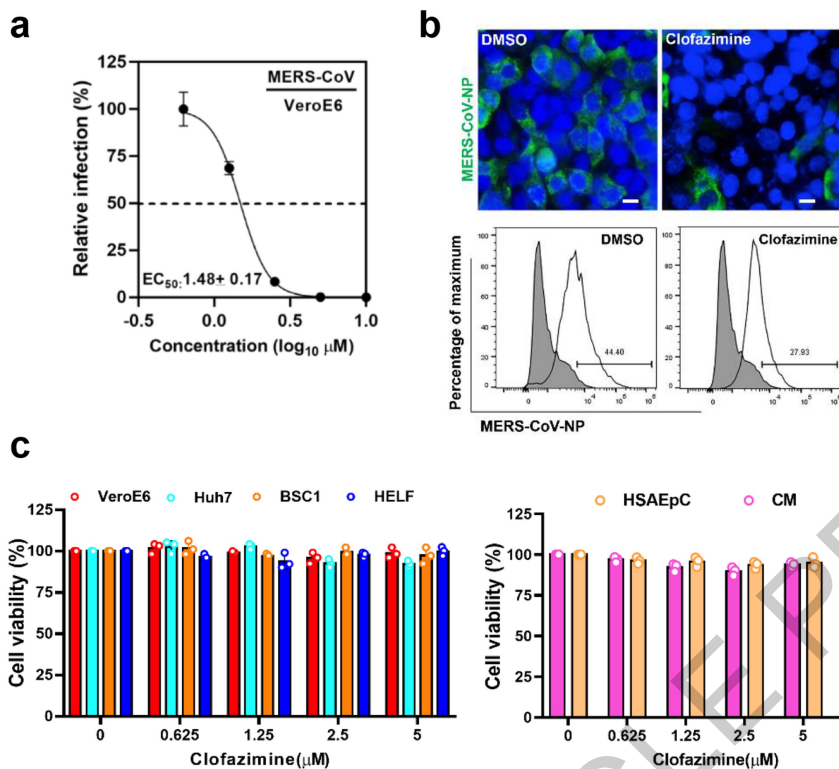
Additional information

Supplementary information The online version contains supplementary material available at <https://doi.org/10.1038/s41586-021-03431-4>.

Correspondence and requests for materials should be addressed to R.S., S.K.C. or K.-Y.Y.

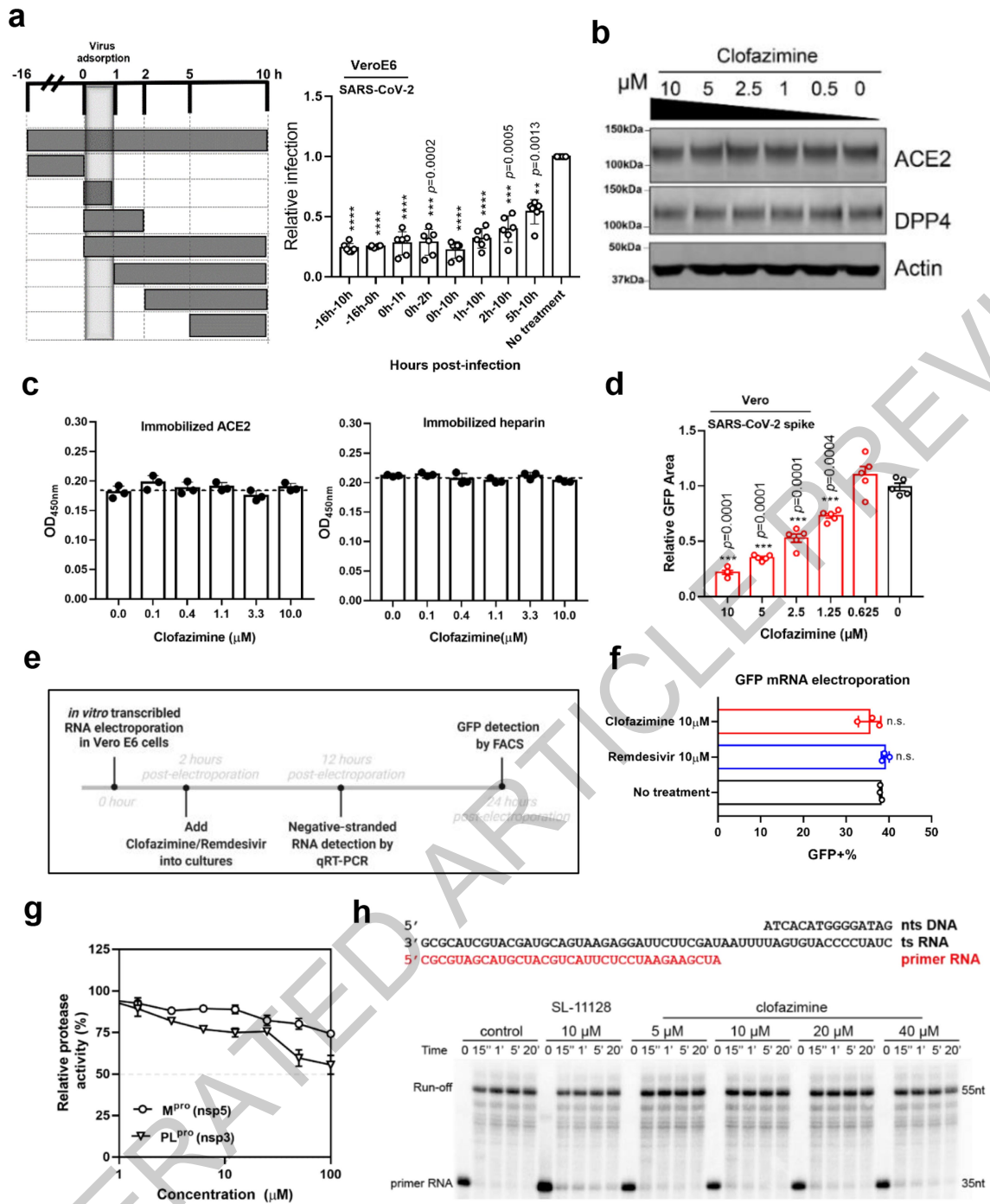
Peer review information Nature thanks the anonymous reviewer(s) for their contribution to the peer review of this work. Peer review reports are available.

Reprints and permissions information is available at <http://www.nature.com/reprints>.



Extended Data Fig. 1 | Anti-MERS-CoV activity and cytotoxicity measurement of clofazimine in matching cells. (a) Clofazimine inhibited MERS-CoV replication in a dose-dependent manner. EC_{50} was achieved by plaque reduction assay and plotted using logistic non-linear regression model (GraphPad Prism 7). Data is shown as mean \pm SD of $n=3$ biologically independent samples. (b) MERS-CoV-infected Huh7 cells (0.01 MOI) were treated with or without clofazimine (5 μM). Upper panel: immunofluorescence staining of MERS-CoV-NP antigen (green), and Huh7 cell nucleus (blue). Scale bar: 20 μm . Shown are representative images selected from a pool images captured in two independent experiments. Lower panel: MERS-CoV-NP

positive cells quantitated by flow cytometry. The experiments were performed twice with representative quantifications shown. (c) The cell viability was determined using CellTiter-Glo assays and in the absence of virus infection. The drug-incubation time in the cytotoxicity assay was consistent with that in the antiviral assay, e.g. at 24h post-treatment for Huh7 cells, primary human small airway epithelial cells (HSAEpC) and human embryonic stem cells-derived cardiomyocytes (CM); at 48h post-treatment for Vero E6 and Caco-2 cells; and at 72h post-treatment for BSC1 and human embryonic lung fibroblasts (HELFL), respectively. Data represent mean \pm SD for $n=3$ biological replicates. The experiment was repeated twice for confirmation.



Extended Data Fig. 2 | See next page for caption.

Article

Extended Data Fig. 2 | Exploration of possible effects of clofazimine on virus entry and replication. (a) Time-of-addition assay. SARS-CoV-2 infected VeroE6 cells were incubated with clofazimine and at time-points indicated. Infection at 10hpi was quantified by immunostaining for NP. Data are normalized to the DMSO-treated and are presented as mean \pm SD for n=6 independent experiments. One-way ANOVA followed by Tukey post-hoc test. (b) Clofazimine has no effect on ACE2 and DPP4 expression. Caco-2 cells were treated with clofazimine for 16 hours prior to collection for western blotting analysis. The expression of ACE2 and DPP4 were determined using anti-ACE2 antibody (Abcam; ab108252; 1:1,000) and anti-DPP4 antibody (Cell Signaling; 67138T; 1:1000), respectively. For gel source data, see Supplementary Figure 1. The experiment was repeated twice for confirmation. (c) Clofazimine has no inhibition on the binding between either ACE2 or heparin and SARS-CoV-2 Spike protein, which are two critical cellular components for viral attachment and infection. Clofazimine was titrated as the indicated concentrations. Dashed line represents binding without inhibitor (i.e. 0 μ M). Data is shown as mean \pm SD of n=3 biologically independent samples. (d) Quantification is based on the GFP positive area using ImageJ software. Error bars represent SEM for n=5 randomly selected images. One-way ANOVA followed by Dunnett post-test. (e) Scheme of *in vitro* transcribed viral RNA replication assay. Vero E6 cells were

electroporated with *in vitro* transcribed viral RNA. At 2h after seeding, the cells were treated with the drug. Negative-stranded RNA was then quantified at 12h post-electroporation. (f) GFP mRNA was utilized as a negative control and its translation, determined at 24h post-electroporation, was not affected by remdesivir or clofazimine. Error bars represent SEM for n=3 independent experiments. n.s. >0.05 when compared with the 0 μ M group by two-tailed student's t-test. (g) Clofazimine shows marginal effect against M^{pro} and PL^{pro} protease activity. Activity of purified SARS-CoV-2 M^{pro} and SARS-CoV-2 PL^{pro} enzymes was measured after adding peptide substrates, respectively. Enzyme activity in the absence (100% activity) and presence of clofazimine were calculated. Data are presented as mean \pm SD of n=3 independent experiments. (h) Clofazimine shows no inhibition on the polymerase activity of nsp7/nsp8/nsp12 RdRp complex. Scaffold used in this *in vitro* transcription inhibition assay is listed in the upper panel. Inhibition effect of clofazimine or SL-11128 to RdRp core complex was analyzed by a primer elongation assay. SL-11128, a selected SARS-CoV-2 inhibitor¹⁵, shows some inhibition effect as time goes by (0, 15 s, 1 min, 5 min and 20 min), while that of clofazimine was minor ranging from 5-40 μ M. All reactions were performed at 30 °C. All the above experiments were repeated twice for confirmation.

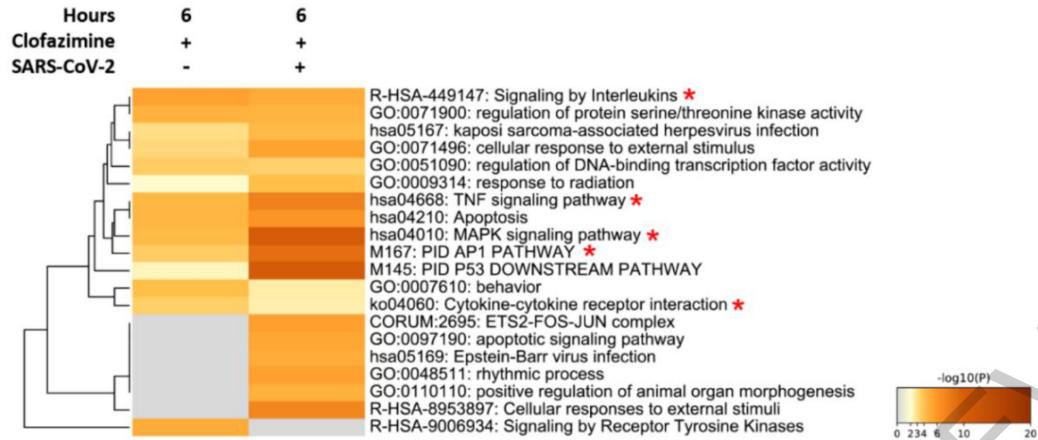
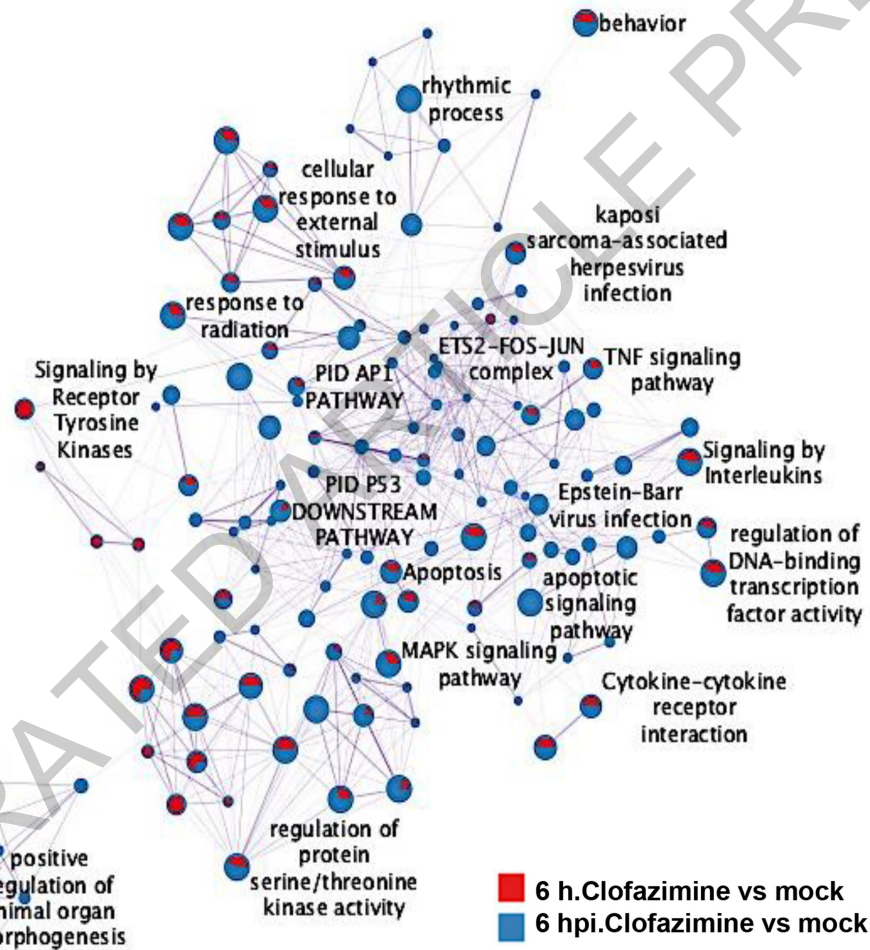
Article

Extended Data Fig. 3 | Transcriptional analysis of clofazimine treatment.

(a) Caco-2 cells were infected with SARS-CoV-2 at MOI of 0.1 before treated with clofazimine, remdesivir and DMSO (0.1%) at the indicated concentrations. Cell culture supernatant was collected at 48hpi and subjected to viral load determination. Two-tailed student's t-test as compared with the DMSO group. * $p < 0.05$, ** $p < 0.01$. Data is shown as mean \pm SD of $n=3$ independent experiments. (b) Timeline of the transcriptomic study (MOI=4). h=hours after drug treatment; hpi=hours post virus infection; CFZ = clofazimine. (c) PCA analysis of RNA-seq dataset after RPKM (Reads Per Kilobase of transcript per Million reads mapped) normalization on each gene expression level. Each dot represents one sample. The percentage labelled on the x or y axis represents the proportion of variance explained with each principal component (PC).

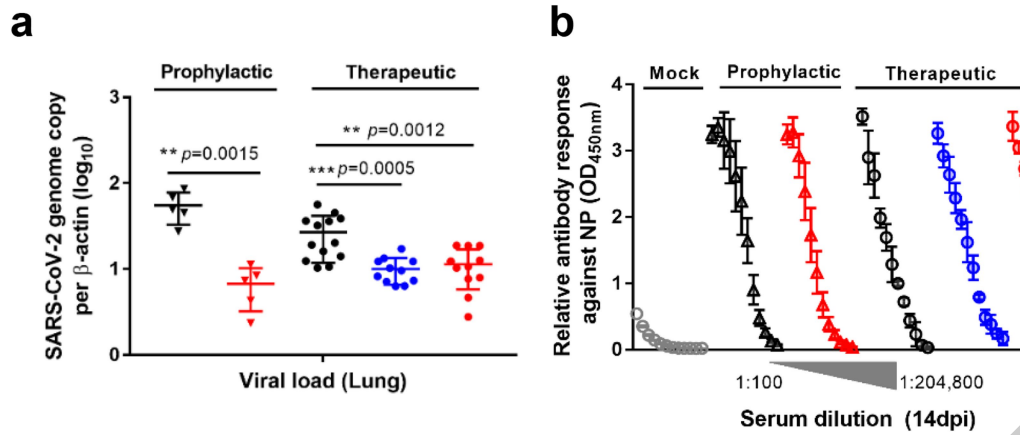
(d) Patterns of transcription levels across all samples. The genes that were significantly and differentially expressed (fold change >2 or <0.5 , FDR <0.05) between 6 hpi and mock are shown. Conditions include 3 hpi and 6 hpi of Caco-2 cells post infection, MOI=4, with/without clofazimine treatment. Genes were clustered by K-means method. (e) Heatmap of 197 transcription factors regulated by clofazimine treatment without infection (left panel), and known interactions among these transcription factors (right panel). (f) Heat map of the genes enriched in MAPK signaling, TNF signaling, Interleukins (ILs) signaling, or cytokine-cytokine receptor interaction. These genes are up-regulated (fold change >2 , FDR <0.05) by either 6 h. clofazimine (without infection) or 6 hpi. clofazimine (with infection) compared to mock-infection.

ACCELERATED ARTICLE PREVIEW

a**b**

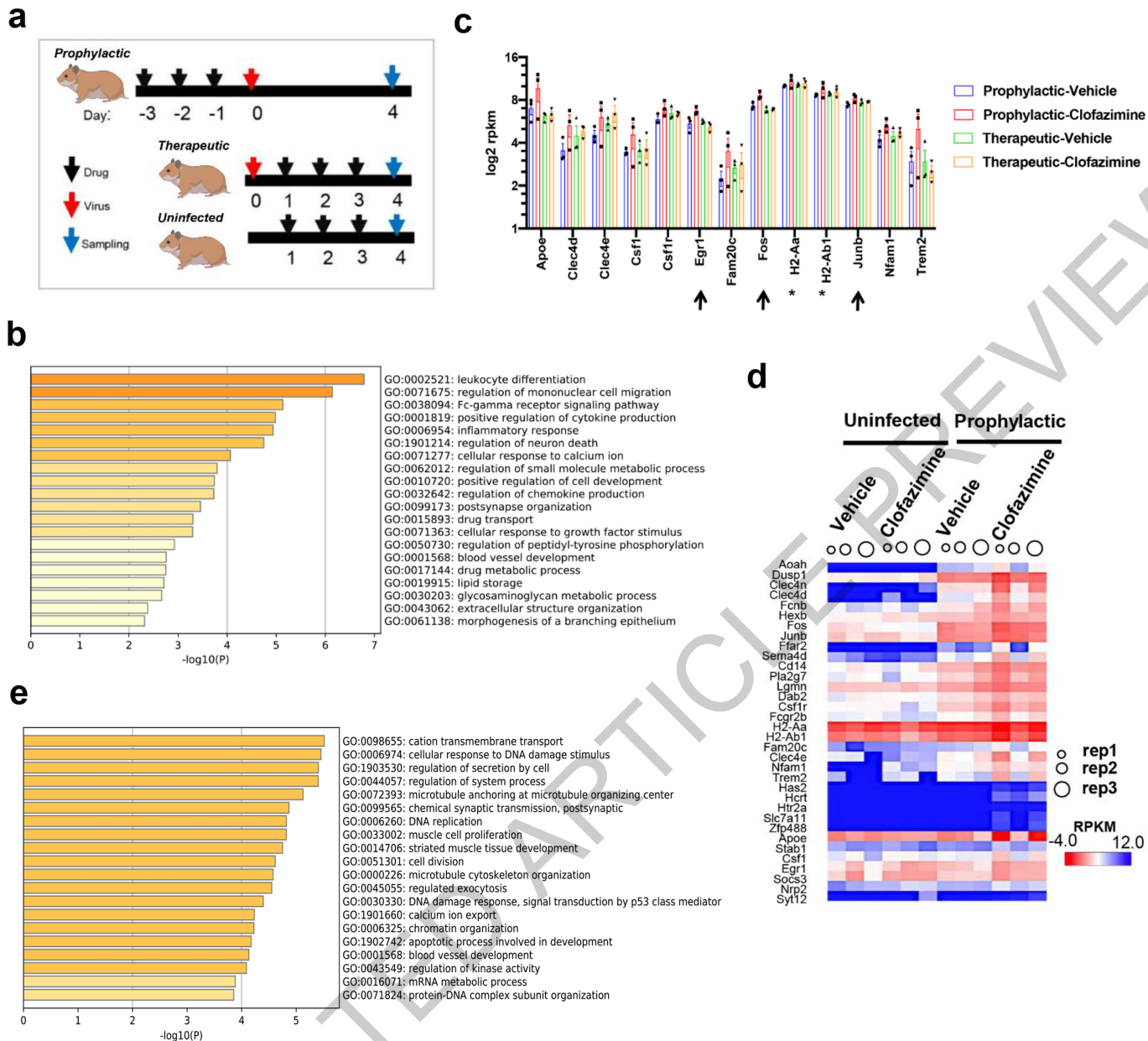
Extended Data Fig. 4 | Transcriptional comparison of clofazimine-treated cells with or without SARS-CoV-2 infection. (a) Top enriched pathways of significantly up-regulated genes (FDR<0.05, fold change >2) compared between clofazimine treatment alone at 6 h versus mock-infected cells (6 h CFZ vs mock) and at 6 hpi under clofazimine treatment versus mock (6 hpi. CFZ vs mock). Pathway analysis was performed by Metascape (* labels innate

immunity related pathways). (b) Network of enriched terms represented as pie charts. Pies are color-coded based on the identities of the gene lists. “6 h. clofazimine vs mock” represents the up-regulated genes by clofazimine treatment without infection at 6 hours and compared with the mock. “6 hpi. Clofazimine vs mock” represents the up-regulated genes by clofazimine treatment at 6 hours post-infection and compared with the mock.



Extended Data Fig. 5 | Prophylactic and therapeutic clofazimine reduced hamster lung viral load without compromising the animal humoral response. Experimental design is shown in Figure 3a. **(a)** Viral yield in the hamster lung tissue, after prophylactic (n=5 animals/group) or therapeutic treatment (n=11 animals for each remdesivir and clofazimine group and n=13 animals for vehicle group), were harvested at 4dpi and titrated by RT-qPCR

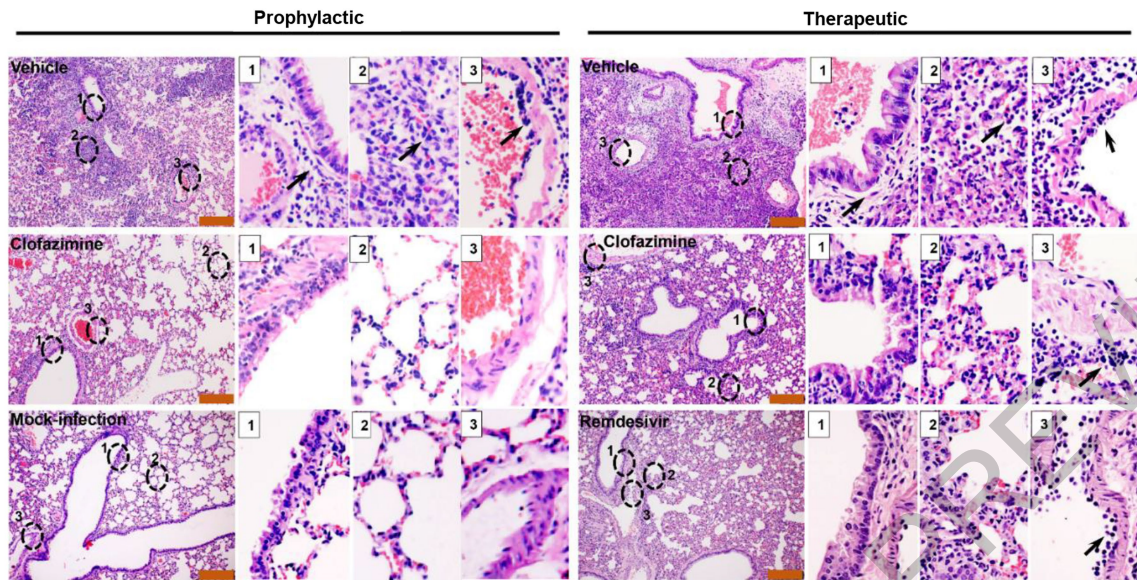
assays. Data are shown as mean \pm SD. Two-tailed student's t-test for prophylaxis groups and one-way ANOVA followed by Dunnett's post-test for therapeutic groups comparing with the vehicle group (black symbols). *** $p<0.001$, ** $p<0.01$. **(b)** Hamsters exhibited normal humoral immune response after SARS-CoV-2 infection and clofazimine treatment. The sera were serially diluted before adding to the NP-coated ELISA plate (n=3 animals/group).



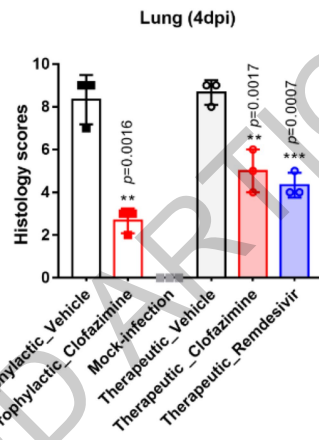
Extended Data Fig. 6 | Transcriptional analysis of hamster lung tissues with clofazimine administration. (a) Experimental design: tissue samples were collected at indicated time points. **(b)** Gene Ontology Biological Process (GO-BP) analysis results on up-regulated genes comparing prophylactic clofazimine administration with its corresponding vehicle controls. **(c)** RNA expression (Reads Per Kilobase of transcript per Million mapped reads, RPKM) of the 13 genes enriched in “Leukocyte differentiation” category of GO-BP analysis. These genes are up-regulated (fold change > 1.5, p value < 0.01) by

prophylactic clofazimine group versus vehicle controls. MHCII molecules were labeled with *. Transcription factors up-regulated by clofazimine on both Caco-2 cells and hamster lung tissues were labeled with †. Data are presented as mean ± SEM of n=3 animals/group. **(d)** Heat map of immune response related genes in uninfected and infected hamster lungs administrated with prophylactic clofazimine or vehicle controls. **(e)** Gene Ontology Biological Process (GO BP) analysis results on up-regulated genes comparing clofazimine and vehicle-treated hamster lungs without virus infection.

a



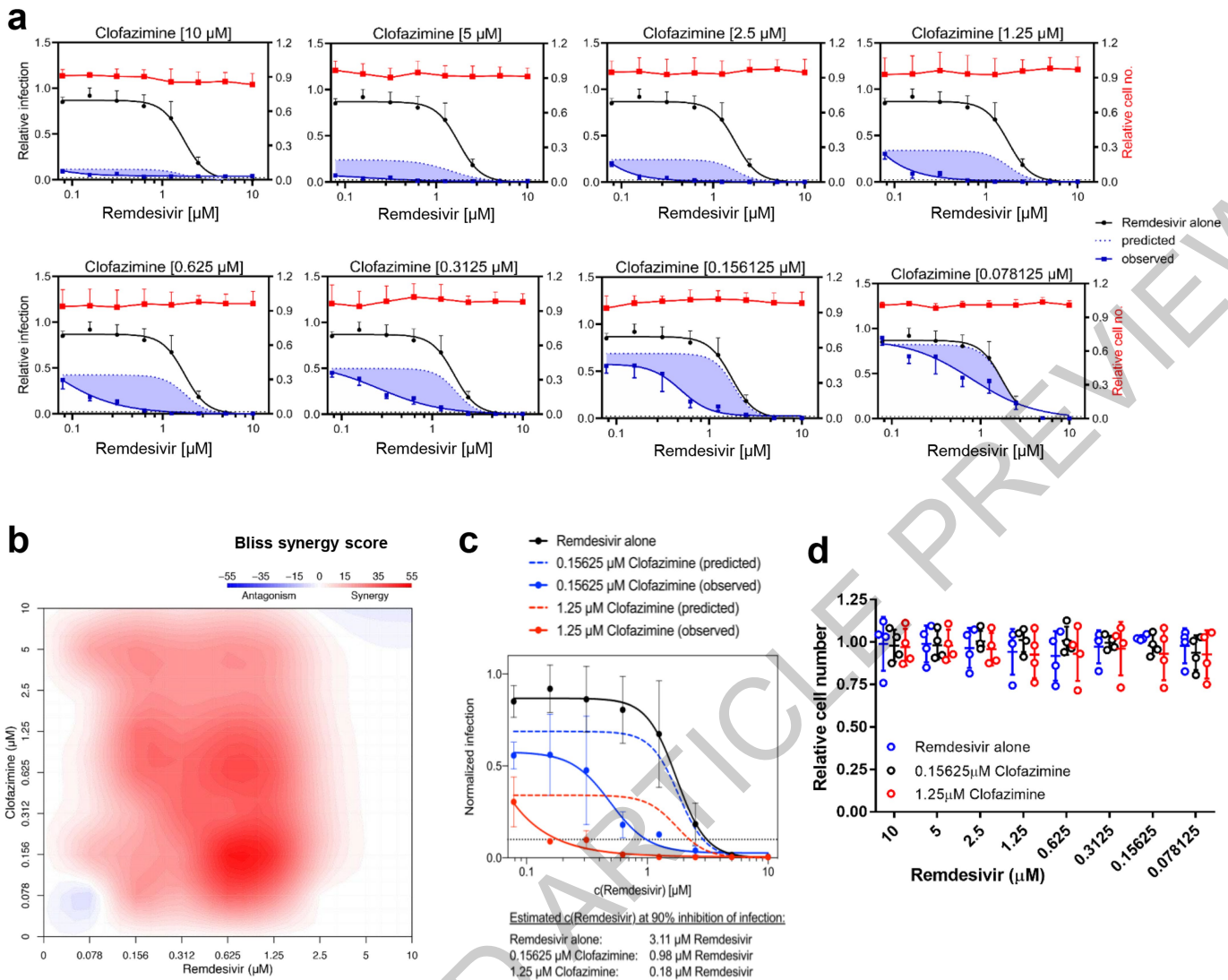
b



Extended Data Fig. 7 | Histological analysis lung pathology in each group.

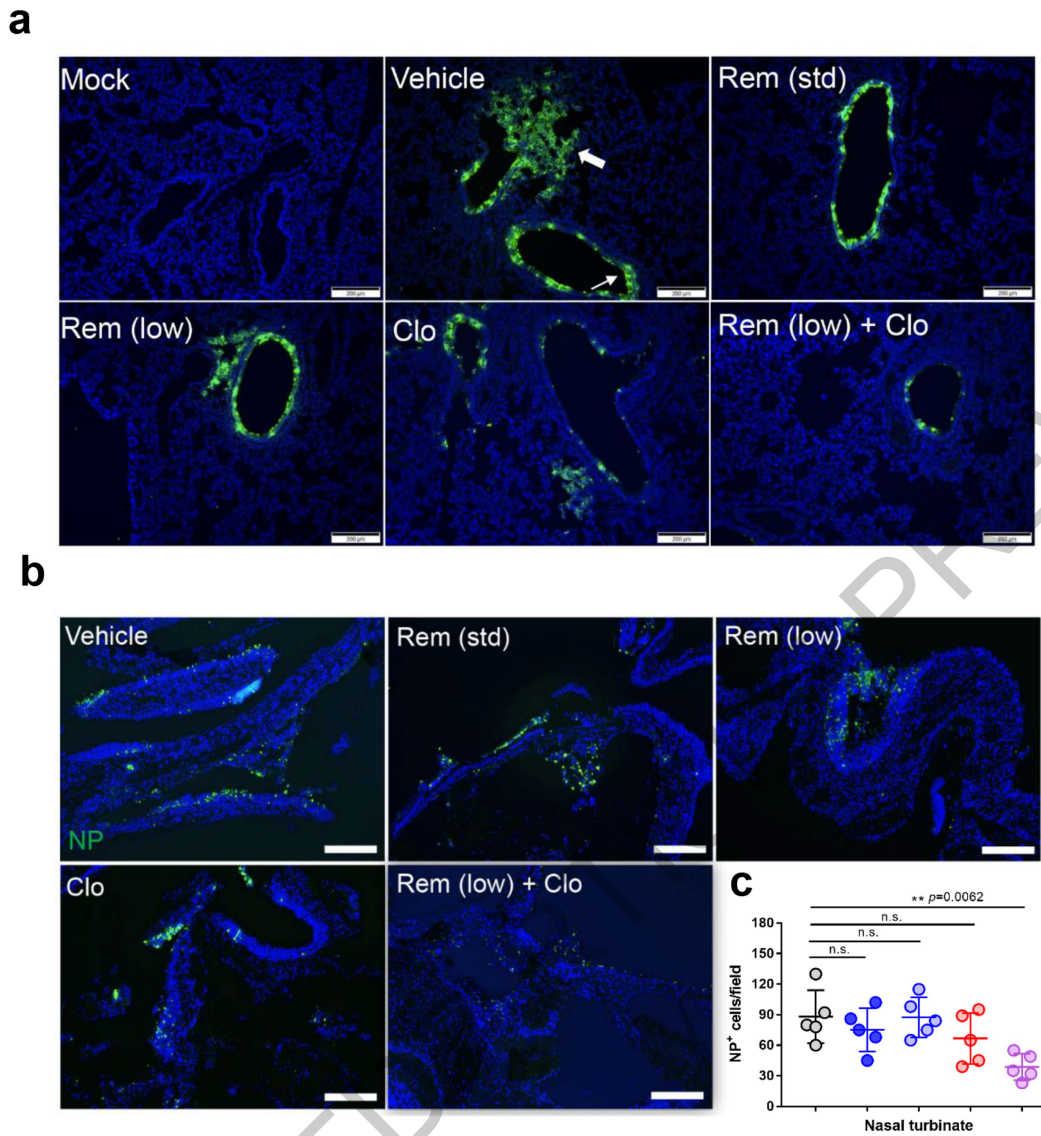
(a) Representative images of H&E-stained lung tissue section from hamsters treated with different groups indicated. Numbered circled areas are shown in magnified images to the right, illustrating the severity of (1) bronchiolar and/or peribronchiolar cell death; (2) alveoli destruction and/or alveolar infiltration; (3) blood vessel and perivascular infiltration. Black arrows indicate sites of infiltrations. These representative images were selected from a pool of 15 images captured in three randomly selected hamsters per group. Scale bar, 200 μ m. (b) A semi-quantitative histology scores were given to each lung tissue through grading the severity of damages in bronchioles, alveoli and blood vessel and accumulating the total scores. Bronchioles: 0=normal structure; 1=mild peribronchiolar infiltration; 2= peribronchiolar infiltration plus

epithelial cell death; 3=score 2 plus intra-bronchiolar wall infiltration and epithelium desquamation. Alveoli: 0=normal structure; 1=alveolar wall thicken and congestion; 2=focal alveolar space infiltration or exudation; 3=diffuse alveolar space infiltration or exudation or haemorrhage. Blood vessel: 0=normal structure; 1=mild perivascular edema or infiltration; 2=vessel wall infiltration; 3=severe endothelium infiltration. Data shown are means \pm SD of three randomly selected slides of each group. Unpaired two-tailed Student's t-test between the two prophylactic groups. One-way ANOVA followed by Dunnett post-test for the therapeutic groups. **p < 0. 01 and ***p < 0.001 when compared with the vehicle control group. Histological score of mock infection was set as zero.



Extended Data Fig. 8 | Clofazimine exhibits antiviral synergy with remdesivir *in vitro*. (a) Remdesivir at indicated doses was combined with clofazimine at indicated doses or a negative control (DMSO), and antiviral dose–response relationships were determined. Vero E6 were pre-treated for 16 h with increasing concentrations of the indicated compound and then infected with SARS-CoV-2 at a MOI of 0.01. Thirty hours after infection, the infected cells were analyzed by immunofluorescence imaging. For each condition, the percentage of infection was calculated as the ratio of the number of infected cells stained for SARS-CoV-2 NP protein to number of cells stained with DAPI. Data are normalized to mean values for DMSO-treated wells and represent mean \pm SEM of $n=4$ biological repeats over 2 independent experiments. (b) Topographic two-dimensional map of synergy scores

determined in synergy finder⁴⁶. Color gradient indicates synergy score (red–highest score). X-axis: remdesivir up to 10 μM, y-axis: clofazimine up to 10 μM. (c) Dose response analysis of remdesivir alone (black) and in combination with 0.15625 μM (blue) or 0.625 μM (red) clofazimine. The observed compound activities are represented by solid lines, while the predicted additive combinatorial activities are indicated by dashed lines. The dotted black line denotes 90% inhibition of infection. Data are normalized to mean values for DMSO-treated wells and represent mean \pm SEM of $n=4$ biological repeats over 2 independent experiments. (d) Counting of cell numbers in each drug combination as indicated. Shown is mean \pm SD of $n=4$ biologically independent samples. The experiments were repeated twice for confirmation.



Extended Data Fig. 9 | Clofazimine exhibits antiviral synergy with remdesivir in hamsters. Experiments were performed as shown in Figure 4b. **(a)** Representative image of infected cells by immunofluorescence staining in lung at 4 dpi. SARS-CoV-2 N protein expression (green) is shown in diffuse alveolar areas (thick white arrow) and in the focal bronchiolar epithelial cells (thin white arrow) of the vehicle-treated hamster lungs, whereas standard and low dosing remdesivir (Rem) groups as well as clofazimine group (Clo) exhibit reduced N expression. Combinatorial therapy restricts the virus replication within the entry gate of lung infection, i.e. bronchiolar epithelial cells. These

representative images were selected from a pool of 15 images captured in three randomly selected hamsters per group. **(b)** Representative image of infected cells by immunofluorescence staining in nasal turbinate at 4 dpi. SARS-CoV-2 N protein (NP) (green) and cell nuclei (blue) were stained. Scale bar 200 μ m. These representative images were selected from a pool of 15 images captured in five hamsters per group. **(c)** NP positive cells per 50 \times field per hamster's nasal turbinate section. One-way ANOVA followed by Dunnett post-test and compared with the vehicle (n=5 animals/group). ** $p < 0.01$ and n.s. indicates non-significant.

Reporting Summary

Nature Research wishes to improve the reproducibility of the work that we publish. This form provides structure for consistency and transparency in reporting. For further information on Nature Research policies, see our [Editorial Policies](#) and the [Editorial Policy Checklist](#).

Statistics

For all statistical analyses, confirm that the following items are present in the figure legend, table legend, main text, or Methods section.

n/a Confirmed

- | | | |
|-------------------------------------|-------------------------------------|--|
| <input type="checkbox"/> | <input checked="" type="checkbox"/> | The exact sample size (n) for each experimental group/condition, given as a discrete number and unit of measurement |
| <input type="checkbox"/> | <input checked="" type="checkbox"/> | A statement on whether measurements were taken from distinct samples or whether the same sample was measured repeatedly |
| <input type="checkbox"/> | <input checked="" type="checkbox"/> | The statistical test(s) used AND whether they are one- or two-sided
<i>Only common tests should be described solely by name; describe more complex techniques in the Methods section.</i> |
| <input checked="" type="checkbox"/> | <input type="checkbox"/> | A description of all covariates tested |
| <input checked="" type="checkbox"/> | <input type="checkbox"/> | A description of any assumptions or corrections, such as tests of normality and adjustment for multiple comparisons |
| <input type="checkbox"/> | <input checked="" type="checkbox"/> | A full description of the statistical parameters including central tendency (e.g. means) or other basic estimates (e.g. regression coefficient) AND variation (e.g. standard deviation) or associated estimates of uncertainty (e.g. confidence intervals) |
| <input type="checkbox"/> | <input checked="" type="checkbox"/> | For null hypothesis testing, the test statistic (e.g. F , t , r) with confidence intervals, effect sizes, degrees of freedom and P value noted
<i>Give P values as exact values whenever suitable.</i> |
| <input checked="" type="checkbox"/> | <input type="checkbox"/> | For Bayesian analysis, information on the choice of priors and Markov chain Monte Carlo settings |
| <input checked="" type="checkbox"/> | <input type="checkbox"/> | For hierarchical and complex designs, identification of the appropriate level for tests and full reporting of outcomes |
| <input checked="" type="checkbox"/> | <input type="checkbox"/> | Estimates of effect sizes (e.g. Cohen's d , Pearson's r), indicating how they were calculated |

Our web collection on [statistics for biologists](#) contains articles on many of the points above.

Software and code

Policy information about [availability of computer code](#)

Data collection

Data analysis

For manuscripts utilizing custom algorithms or software that are central to the research but not yet described in published literature, software must be made available to editors and reviewers. We strongly encourage code deposition in a community repository (e.g. GitHub). See the Nature Research [guidelines for submitting code & software](#) for further information.

Data

Policy information about [availability of data](#)

All manuscripts must include a [data availability statement](#). This statement should provide the following information, where applicable:

- Accession codes, unique identifiers, or web links for publicly available datasets
- A list of figures that have associated raw data
- A description of any restrictions on data availability

Complete sequences of SARS-CoV-2 HKU-001a and SARS-CoV-2 USA-WA1/2020 are available through GenBank (accession numbers MT230904 (HKU-001a), MT246667 and MN908947 (USA-WA1/2020)). The raw RNA-Seq data discussed in this publication have been deposited in NCBI's Gene Expression Omnibus and are accessible through GEO Series accession number GSE162899. The hg38 reference genome is downloaded from UCSC database (<https://hgdownload.soe.ucsc.edu/goldenPath/hg38/bigZips/>). Refseq gene annotation is retrieved from UCSC Table Browser (<https://genome.ucsc.edu/cgi-bin/hgTables>). The NCBI SARS-CoV-2 reference genome (NC_045512.2) is from NCBI database (<https://www.ncbi.nlm.nih.gov/nuccore/1798174254>). The MesAur1.0 (GCA_000349665.1) and annotation is from Ensembl database (https://asia.ensembl.org/Mesocricetus_auratus/Info/Index).

Field-specific reporting

Please select the one below that is the best fit for your research. If you are not sure, read the appropriate sections before making your selection.

Life sciences Behavioural & social sciences Ecological, evolutionary & environmental sciences

For a reference copy of the document with all sections, see [nature.com/documents/nr-reporting-summary-flat.pdf](https://www.nature.com/documents/nr-reporting-summary-flat.pdf)

Life sciences study design

All studies must disclose on these points even when the disclosure is negative.

Sample size	Sample size is chosen based on the standard of the corresponding field. The sample size for each experiment is specified in each corresponding figure legend. Vero E6, Caco2, BSC1, HELF and Huh-7 cell lines were used in this study and n= at least 3 independent experiments were performed. For hPSC-derived cardiomyocytes, primary small airway epithelial cells, experiments were performed with n=3. For ex vivo tissue lung samples, experiments were performed with n=5. For the animal study using golden Syrian hamsters for SARS-CoV-2 infection, a sample size of at least more than 5 was selected to evaluate the level of variation between individuals.
Data exclusions	No data has been excluded from the analyses presented in this manuscript.
Replication	In order to verify the reproducibility of the experimental findings, all the studies in cell models were performed at least in duplicate and the means +/- SEM or SD as well as the nature of 'n' are indicated in the figure legends. All replication attempts were successful and no data was excluded from the analyses.
Randomization	For ex vivo study, tissue from the donor were divided into several and similar pieces before randomly allocated to each group. For in vivo study, hamsters from different litters were randomly allocated into experimental groups.
Blinding	For animal study, blinding was not applicable because each drug was delivered via different routes of administration. For in vitro studies, blinding is not relevant to our study because the experiments for different groups are carried out in parallel using the same set of protocols and the experimental results are quantitative.

Reporting for specific materials, systems and methods

We require information from authors about some types of materials, experimental systems and methods used in many studies. Here, indicate whether each material, system or method listed is relevant to your study. If you are not sure if a list item applies to your research, read the appropriate section before selecting a response.

Materials & experimental systems

n/a	Involved in the study
<input type="checkbox"/>	<input checked="" type="checkbox"/> Antibodies
<input type="checkbox"/>	<input checked="" type="checkbox"/> Eukaryotic cell lines
<input checked="" type="checkbox"/>	<input type="checkbox"/> Palaeontology and archaeology
<input type="checkbox"/>	<input checked="" type="checkbox"/> Animals and other organisms
<input type="checkbox"/>	<input checked="" type="checkbox"/> Human research participants
<input checked="" type="checkbox"/>	<input type="checkbox"/> Clinical data
<input checked="" type="checkbox"/>	<input type="checkbox"/> Dual use research of concern

Methods

n/a	Involved in the study
<input checked="" type="checkbox"/>	<input type="checkbox"/> ChIP-seq
<input type="checkbox"/>	<input checked="" type="checkbox"/> Flow cytometry
<input checked="" type="checkbox"/>	<input type="checkbox"/> MRI-based neuroimaging

Antibodies

Antibodies used	Rabbit-anti-SARS-CoV-2 nucleoprotein polyclonal antibodies were generated from rabbit immunized with recombinant SARS-CoV-2 nucleoprotein. Rabbit-anti-MERS-CoV nucleoprotein polyclonal antibodies were generated from rabbit immunized with recombinant MERS-CoV nucleoprotein. Anti-VSV-G antibody was generated from I1-Hybridoma (ATCC® CRL-2700™) (1:100). Rabbit-anti-DPP4 antibody (Cell Signaling, USA; Catalog # 67138T) (1:1,000). Rabbit-anti-ACE2 antibody (Abcam, USA; Catalog # ab108252) (1:1,000). Horseradish-peroxidase-conjugated rabbit anti-hamster IgG antibody (Thermo Fisher Scientific, USA; Catalog # A18895)(1:2,000).
Validation	The antibody was tested for cross-reactivity with SARS-CoV2 in Vero E6 cells. The antibody showed specificity to SARS-CoV-2-infected cells and no background in non-infected cells. The antibody against MERS-CoV NP was validated by western blot. Anti-VSV-G antibody (I1, mouse hybridoma supernatant from CRL-2700; ATCC) was used in Hoffmann M, et al. 2020. Cell. 181:271; Edwards M, et al. 2020. J Biol Chem. 295:15174 for inactivating residual VSV-G–pseudotyped virions. Rabbit-anti-DPP4 antibody (Cell Signaling, USA; Catalog # 67138T) was validated by the manufacturer for western blotting and used in Li L, et al. 2019. Mol Med Rep. 20: 445. Rabbit-anti-ACE2 antibody (Abcam, USA; Catalog # ab108252) was validated by the manufacturer for western blotting and used in Sun S, et al. 2020. Cell Host Microbe. 28:124.

Eukaryotic cell lines

Policy information about [cell lines](#)

Cell line source(s)	Vero E6 ,Caco2, BSC1 cells were obtained from ATCC (ATCC® CRL-1586 , ATCC®CRL-HTB-37 and ATCC® CCL-26 respectively). Huh-7 were obtained from Apath LLC (JCRB, 0403) and BHK-21/WI-2 cells from Kerafast. Human embryonic stem cell HES2 was purchased from ESI. Human embryonic lung fibroblasts (HELFL) were developed in house. Human primary small airway epithelial cells were purchased from (HSAEpC, ATCC®PCS-301-010).
Authentication	The commercially available cell lines have not been authenticated after receiving them.
Mycoplasma contamination	All cells were tested negative for mycoplasma contamination.
Commonly misidentified lines (See ICLAC register)	No commonly misidentified cell lines were used in this study.

Animals and other organisms

Policy information about [studies involving animals](#); [ARRIVE guidelines](#) recommended for reporting animal research

Laboratory animals	Male and female Syrian hamster, aged 6-10 weeks old, was involved in the study.
Wild animals	This study did not involve wild animals.
Field-collected samples	The study did not involve samples collected from the field.
Ethics oversight	All experimental protocols were approved by the Animal Ethics Committee in the University of Hong Kong (CULATR) and were performed according to the standard operating procedures of the biosafety level 3 animal facilities (Reference code: CULATR 5370-20).

Note that full information on the approval of the study protocol must also be provided in the manuscript.

Human research participants

Policy information about [studies involving human research participants](#)

Population characteristics	Explant lung tissues were derived from normal human lungs from surgical resections of a 6-year old female, a 9-year old male and a 51-year old female, respectively.
Recruitment	No patients were recruited for this study. Biopsy samples that would have been otherwise discarded were used for experimental analyses.
Ethics oversight	The donors gave written consent as approved by the Institutional Review Board of the University of Hong Kong/Hospital Authority Hong Kong West Cluster (UW13-364).

Note that full information on the approval of the study protocol must also be provided in the manuscript.

Flow Cytometry

Plots

Confirm that:

- The axis labels state the marker and fluorochrome used (e.g. CD4-FITC).
- The axis scales are clearly visible. Include numbers along axes only for bottom left plot of group (a 'group' is an analysis of identical markers).
- All plots are contour plots with outliers or pseudocolor plots.
- A numerical value for number of cells or percentage (with statistics) is provided.

Methodology

Sample preparation	Cells were detached from the culture plate using 1ml of enzyme-free dissociation buffer (Sigma) and fixed by adding 1ml of 10% formaldehyde for 24h at room temperature. Cells were washed once by with Perm/Wash buffer (BD) and stained for the MERS NP polyclonal antibody and then secondary antibody. After 1h incubation at room temperature, cells were washed in phosphate buffered saline supplemented with 2mM EDTA once and resuspended in 200 microliter for analysis.
Instrument	BD FACSCanto™ II Cell Analyzer
Software	FlowJo (v10.0.7)

Cell population abundance

Flow cytometry to quantitate virus-infected cells but did not sort them. Therefore the question for post sort abundance is actually irrelevant.

Gating strategy

All cells were selected in a plot in which FSC-H was plotted versus SSC-H. Within this gate, virus-positive cells were quantified.

Tick this box to confirm that a figure exemplifying the gating strategy is provided in the Supplementary Information.